NASA TN D-1363

TECHNICAL NOTE

D-1363

WIND-TUNNEL INVESTIGATION OF THE DRAG AND STATIC STABILITY CHARACTERISTICS OF FOUR HELICOPTER FUSELAGE MODELS

By George E. Sweet and Julian L. Jenkins, Jr.

Langley Research Center
Langley Station, Hampton, Va.

NATIONAL AERONAUTICS AND SPACE ADMINISTRATION
WASHINGTON
July 1962

NATIONAL AERONAUTICS AND SPACE ADMINISTRATION

TECHNICAL NOTE D-1363

WIND-TUNNEL INVESTIGATION OF THE DRAG AND STATIC STABILITY CHARACTERISTICS OF FOUR HELICOPTER FUSELAGE MODELS

By George E. Sweet and Julian L. Jenkins, Jr.

SUMMARY

Results of an investigation in the Langley 7- by 10-foot wind tunnel to determine the parasite drag characteristics of several helicopter fuselages and fuselage-appendage combinations are presented. Also included are the lateral and longitudinal characteristics of the basic fuselages. Test results of four fuselage shapes, faired and conventional landing skids, and several hub-pylon combinations are presented. These results indicate that, through streamlining, the parasite area of some small helicopters could be reduced by as much as 60 percent. The greatest reductions arise from improvements in landing skid and fuselage design. The largest remaining drag contribution is the hub-pylon installation, which may be 20 to 30 percent of the total configuration drag.

INTRODUCTION

The parasite drag of the helicopter fuselage with its protuberances and appendages absorbs a large portion of the total power required in cruising flight. Since the helicopter has been utilized primarily for low-speed short-range missions, aerodynamic cleanliness has not been of prime importance. (See ref. 1.) Recently, however, the military has expressed a need for a new light observation helicopter with improved cruising efficiency; thus, a high degree of aerodynamic cleanliness is required. It has also been forecast that commercial operations at speeds up to 180 knots would be economical provided low parasite drags are achieved. (See ref. 2.) Available fuselage drag studies exemplify qualities necessary for low fuselage drag. (See refs. 3 to 7.) Also, the benefits of fairing and sealing of minor components have been demonstrated. (See refs. 8 to 10, for example.) Data are available from which the drag of pylons, rotor hubs, various landing gears, and miscellaneous fuselage protuberances can be estimated. (See refs. 11 to 19.) However, some extensions to available information are required inasmuch as these reference data do not provide adequate guidance for either drag or downloads at attitudes peculiar to the helicopter in cruising flight.

The present investigation was made to obtain drag, download, and static stability data over a range of helicopter cruising flight attitudes for several fuselages and appendages. Tests of four fuselages, two landing skids, two rotor hubs, and two variable geometry pylons were made. Basic fuselage measurements of two of the models are compared with results of full-scale tests of the same shapes. (See ref. 20.)

SYMBOLS

All force and moment data are referred to the wind system of axes. The positive sense of forces, moments, and angles is indicated in figure 1.

q	dynamic pressure, $\frac{\rho V^2}{2}$, lb/sq ft
ρ	mass density of air, slug/cu ft
V	free-stream velocity, ft/sec
C_L	lift coefficient, $\frac{F_L}{qbc}$
F_D	drag, lb
F_L	lift, lb
F_C	side force, lb
M_{X_w}	rolling moment, ft-lb
M_{Y_w}	pitching moment, ft-lb
M_{Z_w}	yawing moment, ft-lb
b	span, ft
c	chord, ft
α	angle of attack of fuselage reference line, deg
β	angle of sideslip, deg
Δ	incremental force or moment

APPARATUS AND TESTS

Typical model installations in the Langley 7- by 10-foot wind tunnel are shown in figures 2 and 3.

Models

The fuselages tested were 1/5-scale representations of a four-place light observation helicopter. Basic model dimensions and general characteristics are given in table I. A list of the configurations tested is given in table II.

Description of test fuselages.- Model A (see fig. 4(a)) is generally "fish" shaped and presents airfoil-shaped sections when intersected by horizontal planes parallel to the resultant velocity over the normal range of helicopter cruising attitudes. Model B (fig. 4(b)) represents a minimum wetted area design enclosing the cabin and engine compartments. Models C and D were identical except that model D had an increased cargo volume with a resultant abrupt change in planform. (See fig. 4(c).)

Models A, C, and D were provided with motor-driven rotor shafts for the hub tests. The shaft axis located 1.72 feet from the nose, passed through the assumed center of gravity, and was perpendicular to the fuselage reference line. To insure fixed transition, all models were tested with carborundum transition strips located approximately 6 inches from the nose.

Pylons.- The elements of the rotor support pylons tested are shown in figures 5 and 6. The height of these pylons could be varied so that several hub-fuselage clearances could be simulated. Two basic pylon sizes were tested: one large enough to accommodate engine and transmission; the other wide enough to house only shaft and rotor controls. The base of the wide pylon was also used with the alternate ramp top. (See fig. 6.) Both wide and narrow pylons were designed to Navy No. 1 strut ordinates (ref. 21) and had a fineness ratio of 3.

Rotor hubs.- Two rotor hubs representing conventional and streamlined designs were tested. (See fig. 7.) The discus shape of the faired hub was designed large enough to totally enclose the mechanism of the articulated design. (The resulting hub had 66 percent greater projected frontal area than the articulated design.) Both hubs had stub blades which extended to the 20-percent radius of an assumed rotor, appropriate in size for the models tested. The hubs were rotated at approximately 300 revolutions per minute. There was no appreciable effect of hub rotational speed on the aerodynamic forces as indicated by preliminary tests.

Landing skids.- Figure 8 shows the two types of landing skids tested, tubular and faired. The tubular skids are representative of types in current use. In an effort to reduce the drag of these skids, fairings were added to the tubular support members and all unnecessary junctures and acute angles eliminated as suggested in reference 17. The faired strut sections were set with a 5° positive incidence with respect to the fuselage reference line and the runners of both skids inclined 5° nose down.

Test and Accuracies

All models were tested in their basic configuration and then with various appendages added. These tests were made at an average dynamic pressure of approximately 110 pounds per square foot. This value corresponds to a Reynolds number of about 1.9×10^6 per foot. Forces and moments were measured about three axes with a strain-gage balance mounted within the models. In order to avoid overstressing the balance, it was necessary to add horizontal-tail surfaces to all models. The locations and dimensions of these surfaces are given in table I.

All data presented have been corrected for horizontal buoyancy, solid blockage, and support strut interferences. A stream angle correction to angle of attack (-0.75°) was not applied. The accuracy of the measurements, in terms of full scale, are believed to be as follows:

F_L/q, sq ft	±0.35
F_D/q, sq ft	±0.25
F_C/q, sq ft	±0.30
M_{X_w}/q, cu ft	±0.60
M_{Y_w}/q, cu ft	±5.00
M_{Z_w}/q, cu ft	±2.00
Angle of attack, deg	±0.50
Angle of sideslip, deg	±1.00

Although the overall accuracy of the drag is only ±0.25 square foot, the repeatability of these data is believed to be within ±0.08 square foot.

RESULTS AND DISCUSSION

Presentation of Results

The data presented herein are referred to the wind system of axes with the origin at the center of gravity of the fuselages (1.72 ft from

nose on the fuselage reference line). The positive directions of forces, moments, and angles are shown in figure 1.

Two scales are used for the force and moment data presented; one for the data as measured, the other corresponding to a full-scale helicopter five times larger. These data will be discussed in full-scale terms.

The longitudinal characteristics of the fuselages with and without appendages are presented in figures 9 to 13. The various configurations tested are described in table II. It should be noted that these model characteristics (figs. 9 to 13) include the effects of horizontal-tail surfaces which, for the most part, did not trim fuselage moments to zero. (See fig. 13.) However, calculated horizontal-tail characteristics (fig. 14), based upon the flat-plate data of reference 22, show that this lack of trim does not significantly affect the drag data presented in figures 9 to 12.

Comparisons of the basic fuselage aerodynamic characteristics as affected by angle of attack and sideslip are then shown. (See figs. 15 to 23.) The incremental drag of several different hub-pylon configurations, tested on model A, are compared (fig. 24) and the effect of fuselage shape indicated (fig. 25). Note that all incremental data presented include changes in fuselage aerodynamics in addition to the increment due to the appendage itself. The characteristics of conventional and faired landing skids are discussed (figs. 26 and 27) and then the parasite drag of a small helicopter estimated. Finally, the fuselage characteristics of models C and D are compared with results from full-scale tests of these same shapes. (See fig. 28.)

Basic Fuselages

The characteristics of the basic fuselages, obtained by subtracting calculated horizontal-tail characteristics (fig. 14) from basic fuselage data, are shown in figure 15. (Note that the effects of tunnel stream angle were included in the calculation of the horizontal-tail characteristics.)

The calculated total drag of the fuselages and vertical-tail surfaces, based upon a wetted-area drag coefficient (pp. 6 to 16 of ref. 9), are compared with measured values at $\alpha = 0^{\circ}$ in the following table:

Model	$(F_D/q)_{meas}$	$(F_D/q)_{calc}$
A	0.92	0.89
B	1.20	.79
C	.75	.77
D	1.50	.79

The good agreement between theory and models A and C measurements indicates that pressure drag due to separation is not present. However, pressure drag apparently accounts for a considerable portion of the total drag of models B (34 percent) and D (47 percent). The rapid closure of the fuselage pod of model B to the tail boom is believed to result in flow separation. Note that the expected drag increase by the addition of a pylon to this model was apparently offset by mutual improvement in the flow over the top of the fuselage. (Compare fig. 9(a) with fig. 10(a).) Evidence of flow separation on model D in the region of abrupt planform change (fig. 4(c)) was indicated by tufts as well as the drag measurements. However, full-scale tests of the same shape showed no evidence of flow separation. This result is probably due to the greater Reynolds number of the full-scale tests (about twice that of the present tests). The present tests do suggest, though, the susceptibility of this shape to separation. It should be noted that in both investigations the fuselages were smooth and free of the usual surface defects. Also flow disturbances and distortions due to the presence of a rotor were absent.

Figure 15(b), the variation of fuselage downloads with angle of attack, shows that the lift-curve slopes of fuselages A, B, and C are essentially zero for small angles of attack. Similar results were obtained from tests of a fuselage having deep elliptic sections. (See ref. 23.) The increased width of model D resulted in a lift-curve slope that was about the same as a fuselage having circular cross sections. (See ref. 24.)

The measured slopes of fuselage pitching moments (fig. 15(c)) are compared with theoretical calculations (ref. 25) in the following table:

Model	$\left[\frac{d\left(\frac{M_{Y_W}}{q}\right)}{d\alpha}\right]_{meas}$	$\left[\frac{d\left(\frac{M_{Y_W}}{q}\right)}{d\alpha}\right]_{calc}$
A	3.3	4.8
B	2.9	3.0
C	2.9	4.2
D	3.9	4.4

If these fuselages employ a horizontal tail to trim these moments to zero, some additional drag and appreciably larger downloads can be incurred. (See fig. 16(b).) For example, if a helicopter, utilizing model C or D fuselage design, were traveling at 110 knots in a normal cruise attitude (3° to 6° nose down), downloads of 70 to 100 pounds would be expected. However, these trim downloads could be eliminated by designing the fuselage for zero pitching moments at the expected cruise attitude or possibly by employing a canard rather than a conventional trim surface. (See ref. 26.)

Fuselages in Sideslip

The lateral characteristics of the basic fuselages (horizontal tail on) are shown in figures 17 to 22. Only a 0.2- to 0.3-square-foot increase in drag occurred for the small sideslip angles (2° to 3°) normally encountered in cruise. (See fig. 17.) Sideslip tests of models A and D with appendages added (fig. 23) indicate that any additional interference drag between components due to sideslip is small.

Figure 18 shows that no important changes in lift with sideslip occur for any of the models for the range of angles tested.

The increase of diving moments with increased sideslip (fig. 19) for models A, C, and D is believed to result from fuselage flow interferences on the horizontal tail. A higher aspect ratio tail and/or another tail location may reduce these moment changes.

All test fuselages (vertical tail on) exhibited yaw instability particularly in level and nose-up attitudes. (See fig. 20.) This instability is believed to result primarily from a reduction of the effectiveness of the vertical tail when it is immersed in the flow field of the fuselage.

Calculations of the slopes of the unstable fuselage yawing moments with sideslip (ref. 25) and the stabilizing effect of the vertical tails (ref. 27) are compared in the following table:

Model	$\left[\frac{d\left(\frac{M_{Z_w}}{q}\right)}{d\beta}\right]_{\text{fuselage}}$	$\left[\frac{d\left(\frac{M_{Z_w}}{q}\right)}{d\beta}\right]_{\text{vertical tail}}$
A	-11.8	11.5
B	-7.8	10.0
C and D	-7.5	4.2

Generally, fuselage instability with respect to sideslip increases as the square of local fuselage depth (fuselage width for calculating angle-of-attack stability) and with increasing fineness ratios. (See ref. 25.) Tests of reference 4, for example, showed significantly lower sideslip instability for circular fuselages than for shapes having greater depth.

Rotor Hub and Pylon Drag

Results of drag tests of many different hub designs are available. (See refs. 14 and 15.) The present tests are intended to indicate effects of fuselage hub clearance and angle of attack on drag. These results, obtained on model A fuselage, included tests of conventional and faired rotor hubs on both wide and narrow pylons. (See fig. 24.)

The intermediate hub height (disk plane 21 inches above fuselage) resulted in the least drag for most of the hub-pylon configurations tested. The differences between most of the arrangements tested were small (approximately 0.3 sq ft) except for the ramp-pylon—faired-hub combination. Here, the drag was as much as 0.8 square foot greater than the best configuration. A tuft study of the ramp pylon and faired hub combination indicated that a downward flow emanating from the rear portions of hub and pylon resulted in separation on the fuselage near the pylon base. It is believed that a sizable portion of the measured drag increment of this configuration is due to fuselage pressure drag.

It is important to note that no particular advantage was indicated for the faired hub, the effects of streamlining being offset by increased frontal area and interference velocities. However, the tests of reference 15 demonstrated that the total drag of a conventional three-blade articulated hub can be reduced by approximately 12 percent by merely adding cuff-type fairings over the blade shanks and hub mechanism.

The effect of three fuselage shapes (models A, C, and D) upon the installed drag increment of a particular hub and pylon is shown in figure 25. The largest drag increments occurred on model D as a result of separation on the fuselage.

Landing Skids

The incremental characteristics of the conventional and tubular landing skids are presented in figure 26. The large drag (3.5 sq ft) of the tubular skids was reduced by approximately 63 percent by fairing and relocating the support legs to minimize interference effects. Further reductions are possible through the use of well streamlined sections. (See ref. 20.) The differences between the lift and pitching-moment curves of the tubular skids obtained from tests of models C and D are

believed to arise from airflow differences about the two fuselages. Note the unexpected inverse lift and pitching-moment curves of the faired skids with angle of attack. (See figs. 26(b) and 26(c).) Additional data points from sideslip tests were added to the lift plot to aid in defining the hysteresis present. These reversals and the hysteresis are attributed to the faired support legs and are a function of Reynolds number, nose shape, and fineness ratio. (See ref. 28.)

Appropriate section data for calculating the aerodynamics of the faired skids are not available; however, the section lift of several strut sections (ref. 29) are presented in figure 27 to indicate the effect of Reynolds number and nose shape on force reversal. These reversals, which may be undesirable during maneuvers or landing flares can be easily avoided by selecting a well faired strut section which has a fineness ratio greater than 2.5. (See ref. 30.) An indication of similar force and moment reversals was found during an analysis of the skid tests of reference 20.

Drag Estimate For a Small Helicopter

The equivalent parasite drag of an aerodynamically clean four-passenger helicopter based on representative test results and estimates is indicated in the following table:

Component	$\frac{F_D}{q}$, sq ft	Reference
Fuselage	0.8	Present paper
Hub and pylon	2.0	Present paper
Faired landing skids	1.0	Present paper
Tail rotor power and hub drag	0.8	32
Leakage	0.8	7
Total	5.4	

Note, however, this estimate neglects downloads and increased drag due to actual flight attitudes. In practice some forward shaft tilt (2° to 3°) is frequently used. Hence nose-down attitudes and, consequently, drag and downloads will be reduced. However, a calculation indicates that, for cruise speed of 110 knots, the fuselage would still have to be inclined 3° to 4° nose down in order to minimize rotor flapping motions. At this attitude the configuration drag would be increased by about 0.3 square foot. Allowing for a nominal amount of sideslip (2° to 3°) results in another 0.2 square foot. (See fig. 23.) If the fuselage moments were trimmed to zero with a horizontal tail, the additional rotor power required, expressed in terms of parasite area, is about 0.6 square foot for fuselage C or D and about 0.2 for fuselage A or B. The

resultant parasite area now becomes 6.1 to 6.5 square feet. A more detailed drag estimate (see ref. 20) indicates about 7 square feet for a small helicopter (approximately 2,000 to 2,600 pounds gross weight).

A comparison of this drag estimate with the drag of some current helicopters of comparable size indicates that drag reductions of as much as 60 percent are possible. (See ref. 31.)

Comparison of Model and Full-Scale Data

A comparison of full-scale and 1/5-scale model test results for models C and D is presented in figure 28. Note that the drag of model C, both small and full scale, is in reasonable agreement, as is the lift. However, the drag of model D, 1/5 scale, is nearly twice that of the full-scale model. This difference, as pointed out earlier, results from flow separation on the small model and is related to low Reynolds numbers.

Although the slopes of the pitching-moment curves for both the full-scale and 1/5-scale models agree reasonably well, large differences were found to exist between the angles of attack for zero pitching moments. In an effort to explain these differences a stream angle survey of the Langley 7- by 10-foot tunnel with the model support strut installed was conducted. However, only small stream angle effects, -0.75° α for the fuselages and about -1.0° α for the horizontal tail, were found. As a result the reasons for the moment differences can be only partly explained. The measured data presented herein have not been corrected for tunnel stream angle except for the purpose of comparing 1/5-scale and full-scale model results. (See fig. 28.)

CONCLUDING REMARKS

The reference material listed and the data presented herein have demonstrated that it is feasible to achieve high cruise efficiency for helicopters through drag reduction. Improved landing skid and fuselage streamlining and the avoidance of large downloads can result in appreciable reductions in rotor power requirements. The rotor-hub-pylon installation, however, remains as the largest single drag penalty (about 20 to 30 percent of the total configuration drag). This large drag is of considerable concern, although it is not completely unexpected, as a review of available literature will indicate. Some minor hub drag reduction is indicated through the use of cuff-type fairing and by proper choice of fuselage-hub clearance to minimize interference velocities. It is expected that any major improvement would result only by reducing hub frontal area.

In general, it can be concluded that adherence to good streamlining in the early design stages cannot be substituted for by modifications and fixes in the production helicopter.

Langley Research Center,
National Aeronautics and Space Administration,
Langley Station, Hampton, Va., April 11, 1962.

REFERENCES

1. Bunker, William B.: Design Proposal for a Military Helicopter. Mech. Eng., vol. 74, no. 9, Sept. 1952, pp. 709-715.

2. Brown, E. L., and Drees, Jan M.: Increasing Helicopter Speeds. Proc. Sixteenth Annual National Forum, American Helicopter Soc., Inc., May 1960, pp. 1-10.

3. Markham, John R., and Ober, Shatswell: A Note on Fuselages of Low Drag. Jour. Aero. Sci., vol. 3, no. 8, June 1936, pp. 276-277.

4. Williams, James L.: Wind-Tunnel Investigation of Effects of Fuselage Cross-Sectional Shape, Fuselage Bend, and Vertical-Tail Size on Directional Characteristics of Nonoverlap-Type Helicopter Fuselage Models Without Rotors. NACA TN 3645, 1956.

5. Abbott, Ira H.: Airship Model Tests in the Variable Density Wind Tunnel. NACA Rep. 394, 1931.

6. Diehl, Walter S.: Tests on Airplane Fuselages, Floats, and Hulls. NACA Rep. 236, 1926.

7. Shultz, A. W.: XH-40 Wind Tunnel Test. Part II - Data Analysis. Rep. No. 204-099-752 (Contract No. AF 33(600)30229), Bell Aircraft Corp., Oct. 2, 1956.

8. Lange, Roy H.: A Summary of Drag Results From Recent Langley Full-Scale-Tunnel Tests of Army and Navy Airplanes. NACA WR L-108, 1945. (Formerly NACA ACR L5A30.)

9. Hoerner, Sighard F.: Fluid-Dynamic Drag. Publ. by the author (148 Busteed Drive, Midland Park, N. J.), 1958.

10. Dearborn, C. H., and Silverstein, Abe: Drag Analysis of Single-Engine Military Airplane Tested in the NACA Full-Scale Wind Tunnel. NACA WR L-489, 1940. (Formerly NACA ACR, Oct. 1940.)

11. Harrington, Robert D.: Reduction of Helicopter Parasite Drag. NACA TN 3234, 1954.

12. Foster, R. D.: Results of the 1/2 Scale HU-1 and High Speed Helicopter Pylon and Hub Model Wind Tunnel Investigation. Rep. No. 8025-099-012, Bell Helicopter Co., Mar. 21, 1961.

13. Hickey, David H.: Full-Scale Wind-Tunnel Tests of the Longitudinal Stability and Control Characteristics of the XV-1 Convertiplane in the Autorotating Flight Range. NACA RM A55K21a, 1956.

14. Churchill, Gary B., and Harrington, Robert D.: Parasite-Drag Measurements of Five Helicopter Rotor Hubs. NASA MEMO 1-31-59L, 1959.

15. Jones, J. R., and Lund, P. D.: Full Scale Investigation of Rotor Hub Fairing for a Sikorsky H-5 Rotor Hub. Rep. No. 55McC103R (Contract No. AF 18(600)-176), McCulloch Motors Corp., Apr. 1955. (Available from ASTIA as AD No. 93925.)

16. Herrnstein, William H., Jr., and Bierman, David: The Drag of Airplane Wheels, Wheel Fairings, and Landing Gears - I. NACA Rep. 485, 1934.

17. Bierman, David, and Herrnstein, William H., Jr.: The Interference Between Struts in Various Combinations. NACA Rep. 468, 1933.

18. Abbott, Ira H.: The Drag of Two Streamline Bodies as Affected by Protuberances and Appendages. NACA Rep. 451, 1932.

19. Williams, James L.: Wind-Tunnel Investigation of Effects of Spoiler Location, Spoiler Size, and Fuselage Nose Shape on Directional Characteristics of a Model of a Tandem-Rotor Helicopter Fuselage. NACA TN 4305, 1958.

20. Jenkins, Julian L., Jr., Winston, Matthew M., and Sweet, George E.: A Wind-Tunnel Investigation of the Longitudinal Aerodynamic Characteristics of Two Full-Scale Helicopter Fuselage Models With Appendages. NASA TN D-1364, 1962.

21. Diehl, Walter S.: Engineering Aerodynamics. The Ronald Press Co., 1928.

22. Monteith, Charles N.: Simple Aerodynamics and the Airplane. Third ed., The Ronald Press Co., c.1929.

23. Bates, William R.: Static Stability of Fuselages Having a Relatively Flat Cross Section. NACA TN 3429, 1955. (Supersedes NACA RM L9I06a.)

24. Jacobs, Eastman N., and Ward, Kenneth E.: Interference of Wing and Fuselage From Tests of 209 Combinations in the N.A.C.A. Variable-Density Tunnel. NACA Rep. 540, 1935.

25. Multhopp, H.: Aerodynamics of the Fuselage. NACA TM 1036, 1942.

26. Scallion, William I., and Cannon, Michael D.: The Low-Speed Longitudinal and Lateral Characteristics of a Delta-Wing Model with Fixed and Free-Floating Canard Surfaces. NASA TM X-120, 1959.

27. Perkins, Courtland D., and Hage, Robert E.: Airplane Performance Stability and Control. John Wiley & Sons, Inc., 1949.

28. Polhamus, Edward C.: Effect of Flow Incidence and Reynolds Number on Low-Speed Aerodynamic Characteristics of Several Noncircular Cylinders With Applications to Directional Stability and Spinning. NASA TR R-29, 1959. (Supersedes NACA TN 4176.)

29. Cowley, W. L., Simmons, L. F. G., and Coales, J. D.: An Investigation To Determine the Best Shape of Fairing Piece for a Cylindrical Strut. R & M. No. 256, sec. I, British ACA, 1916.
Jones, R., and Levy, H.: Tests on a Series of Large Struts of Varying Fineness Ratio. R & M. No. 256, sec. II, British ACA, 1916.

30. Thomson, G. P.: Applied Aerodynamics. Hodder and Stoughton Ltd. (London), 1919.

31. Moser, Herbert H.: Full Scale Wind Tunnel Investigation of Helicopter Drag. Jour. American Helicopter Soc., vol. 6, no. 1, Jan. 1961, pp. 27-33.

TABLE I.- GEOMETRIC CHARACTERISTICS OF TEST MODELS

		Model			
		A	B	C	D
Overall length, ft		5.65	5.83	5.82	5.82
Location of rotor shaft and model moment center from nose, ft		1.72	------	1.72	1.72
Rotor hub height above fuselage reference line for narrow, wide, and ramp pylons, ft	Low	0.836	------	0.820	0.820
	Intermediate . .	0.919	------	------	------
	High	1.086	------	------	------
Distance from model moment center to the quarter chord of horizontal tail, ft		3.22	3.22	3.22	3.22
Tail incidence angle with respect to reference line, deg		5± 0.5	0± 0.5	0 ± 0.5	0 ± 0.5
Area of horizontal tail, sq ft		0.194	0.113	0.194	0.194
Projected frontal area of basic model, sq ft		0.757	0.709	0.749	0.791
Volume of basic model, cu ft		2.018	1.558	1.544	1.631

TABLE II.- LIST OF CONFIGURATIONS TESTED

[X denotes value applied]

Configuration	Basic fuselage	Hubs		Pylon elements			Skids		Total frontal area, sq ft
		Faired	Conventional	Wide top	Ramp top	Wide pylon base	Faired	Tubular	
Model A									
	Projected frontal area of -								
	0.757	0.102	0.062	0.055	0.070	0.001	-----	-----	
1	X								0.757
2	X			X		X			.813
3	X		X	X		X			.875
4	X	X		X		X			.915
Model B									
	Projected frontal area of -								
	0.709	-----	-----	0.055	0.070	0.009	-----	-----	
1	X								0.709
2	X			X		X			.773
3	X				X	X			.788
Model C									
	Projected frontal area of -								
	0.749	-----	0.062	0.055	-----	0.017	-----	0.138	
1	X								0.749
2	X			X		X			.821
3	X			X		X		X	.959
4	X		X	X		X		X	1.021
Model D									
	Projected frontal area of -								
	0.791	0.102	0.062	0.055	-----	0.017	0.106	0.138	
1	X								0.791
2	X							X	.929
3	X						X		.897
4	X			X		X	X		.969
5	X		X	X		X	X		1.031
6	X	X		X		X	X		1.071

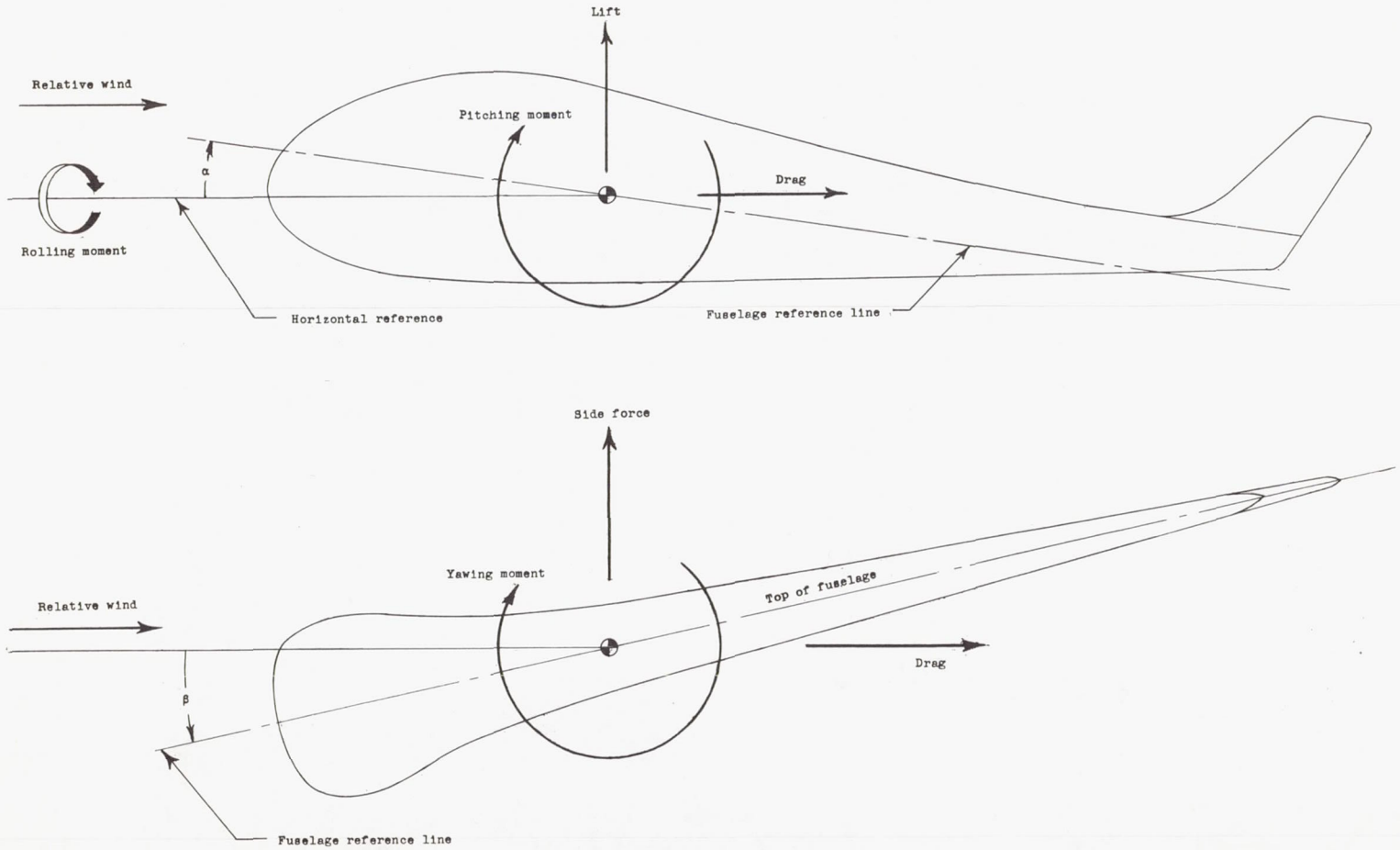

Figure 1.- Axis and force notation showing positive directions of forces and moments.

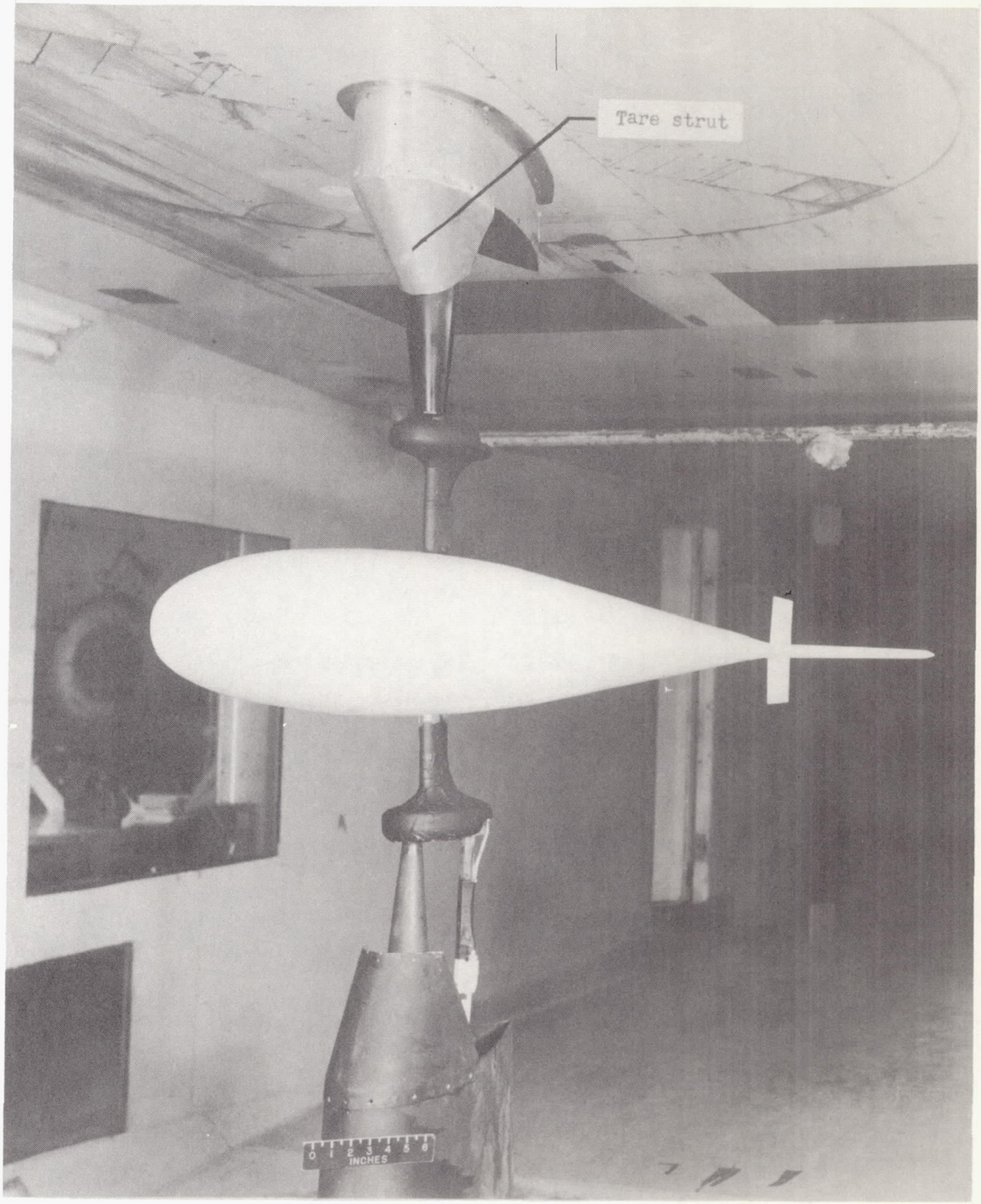

L-60-6580.1

Figure 2.- Model A with tare strut installed, mounted in the Langley 7- by 10-foot wind tunnel.

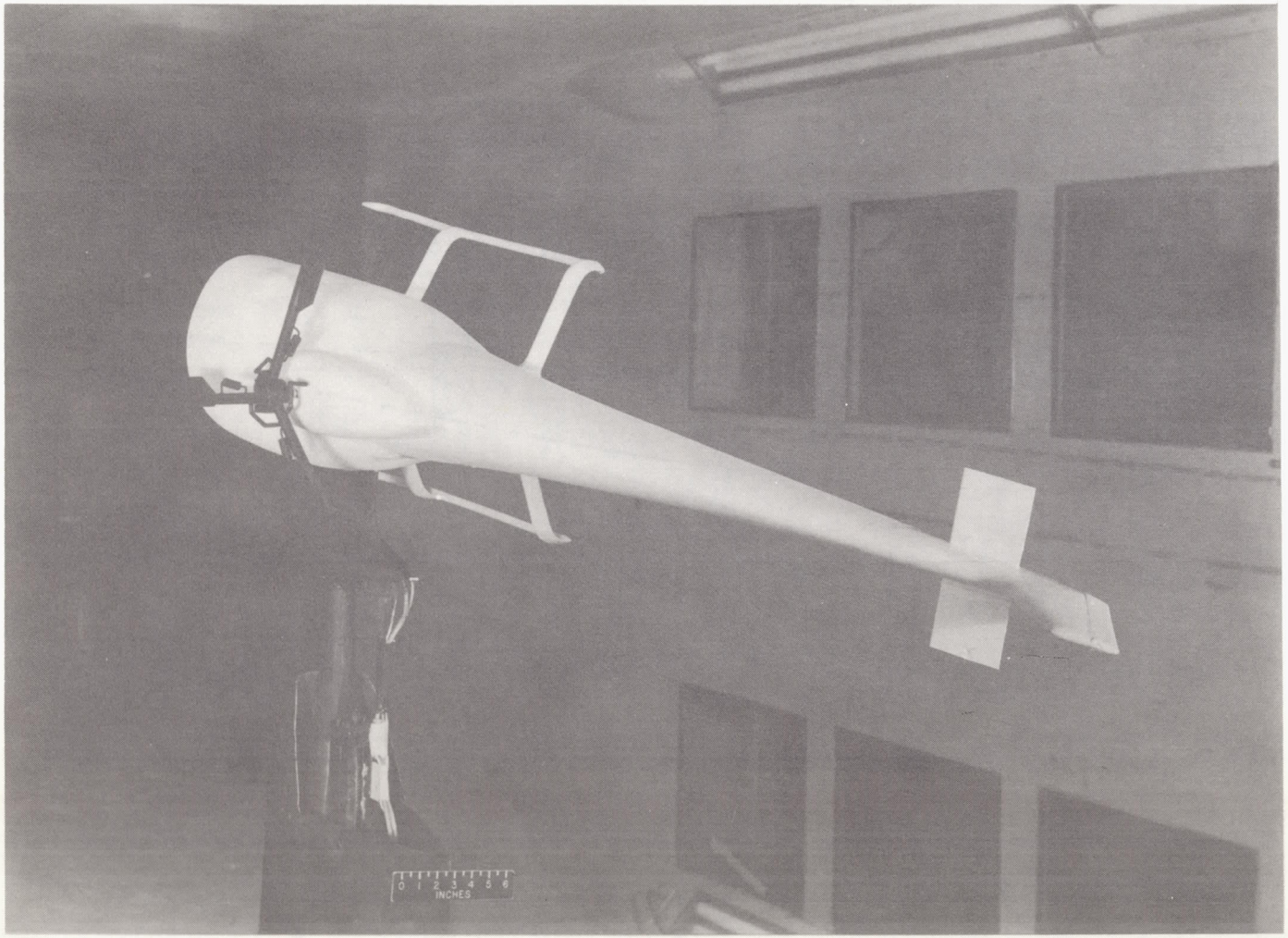

L-60-6583

Figure 3.- Model D with conventional hub and faired landing skids mounted in Langley 7- by 10-foot wind tunnel.

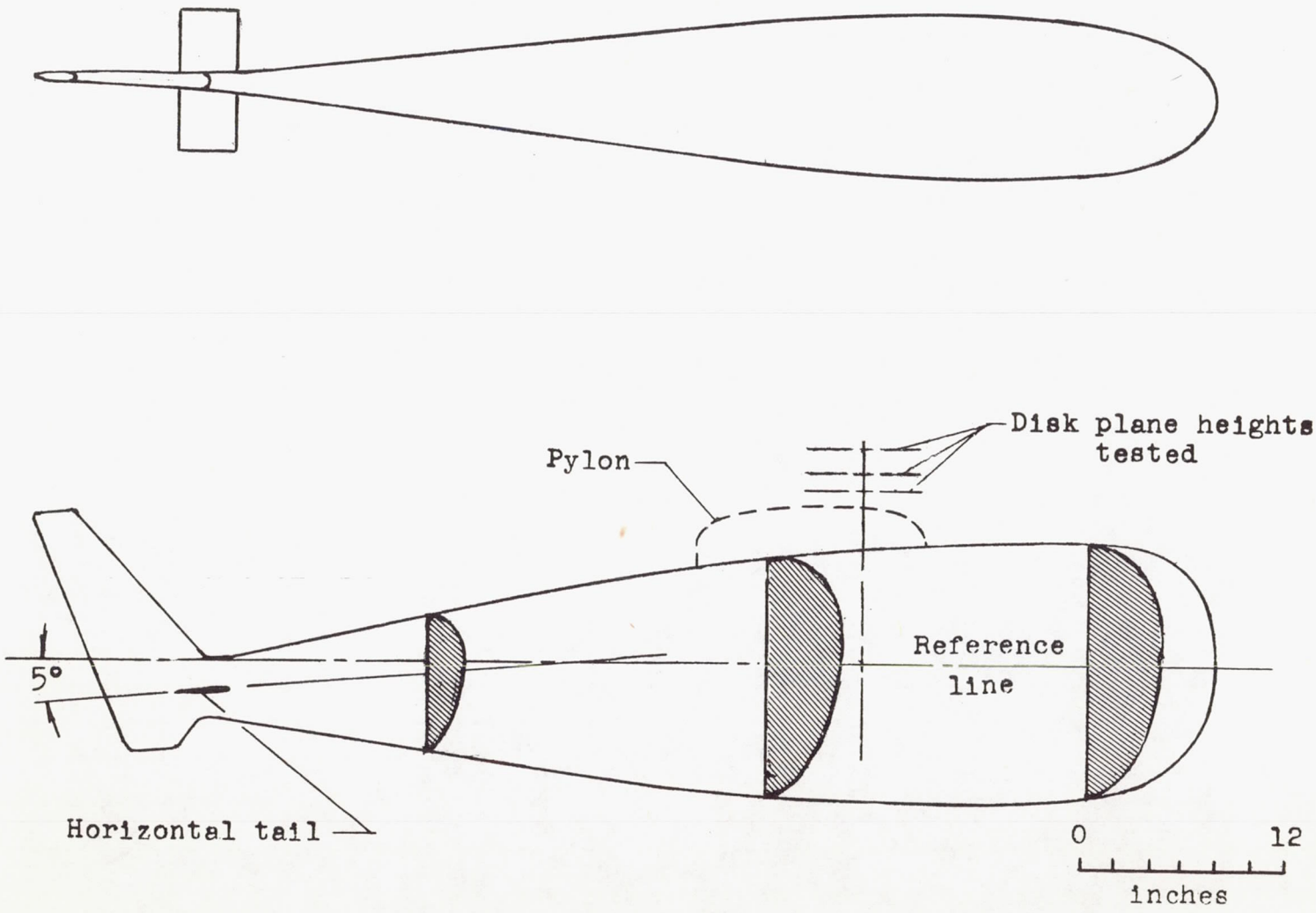

(a) Model A.

Figure 4.- Fuselage models tested.

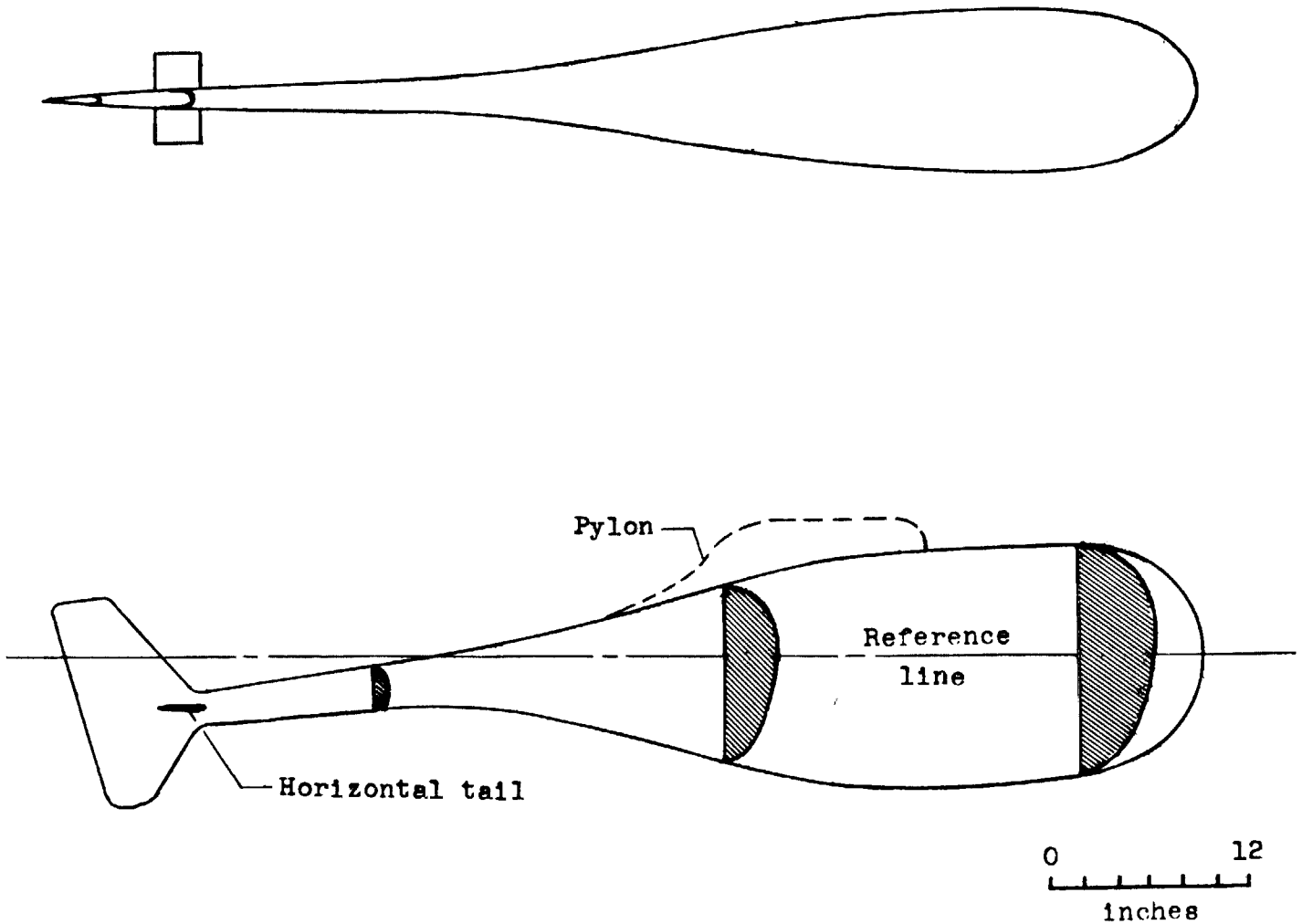

(b) Model B.

Figure 4.- Continued.

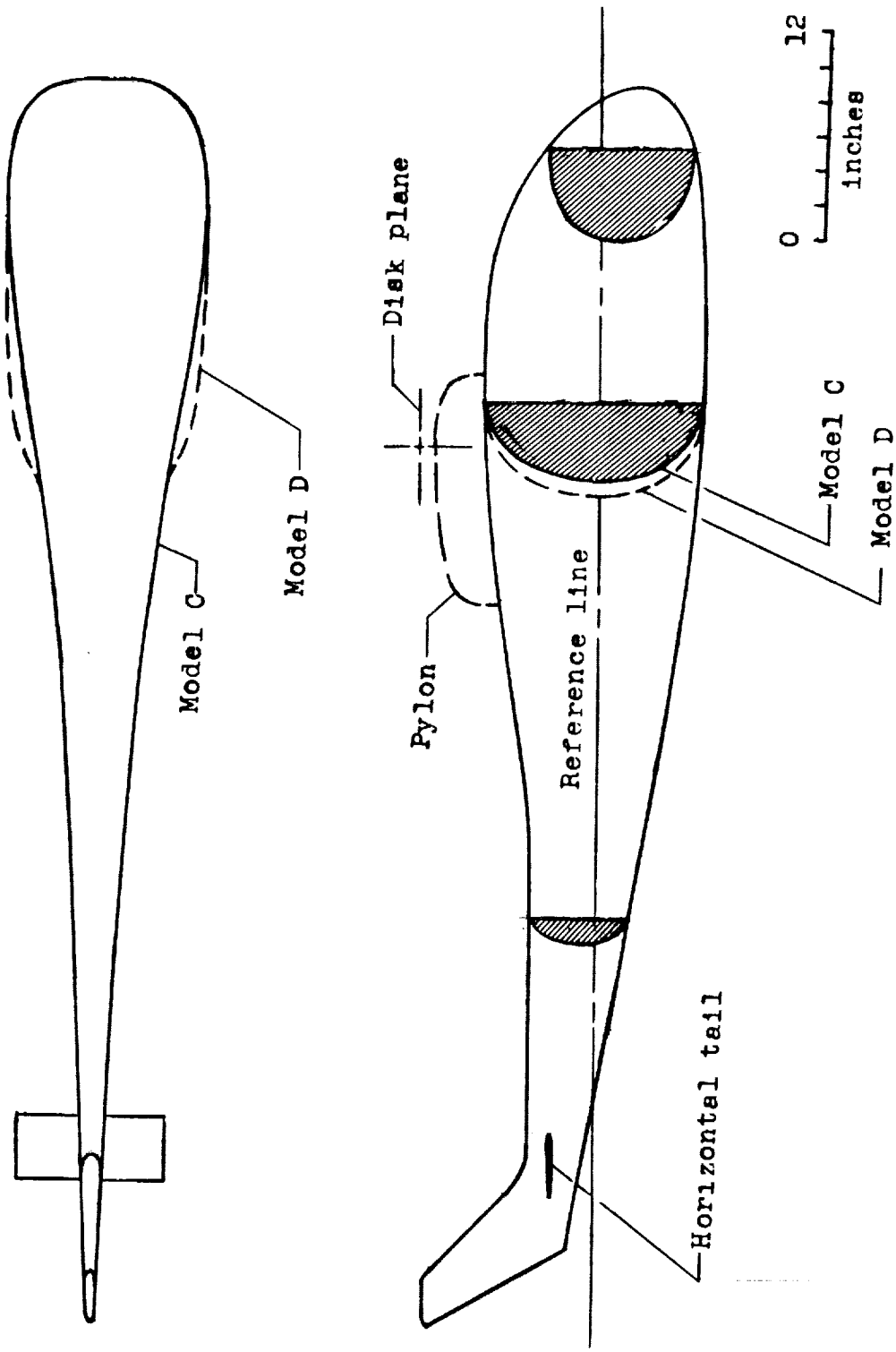

(c) Models C and D.

Figure 4.- Concluded.

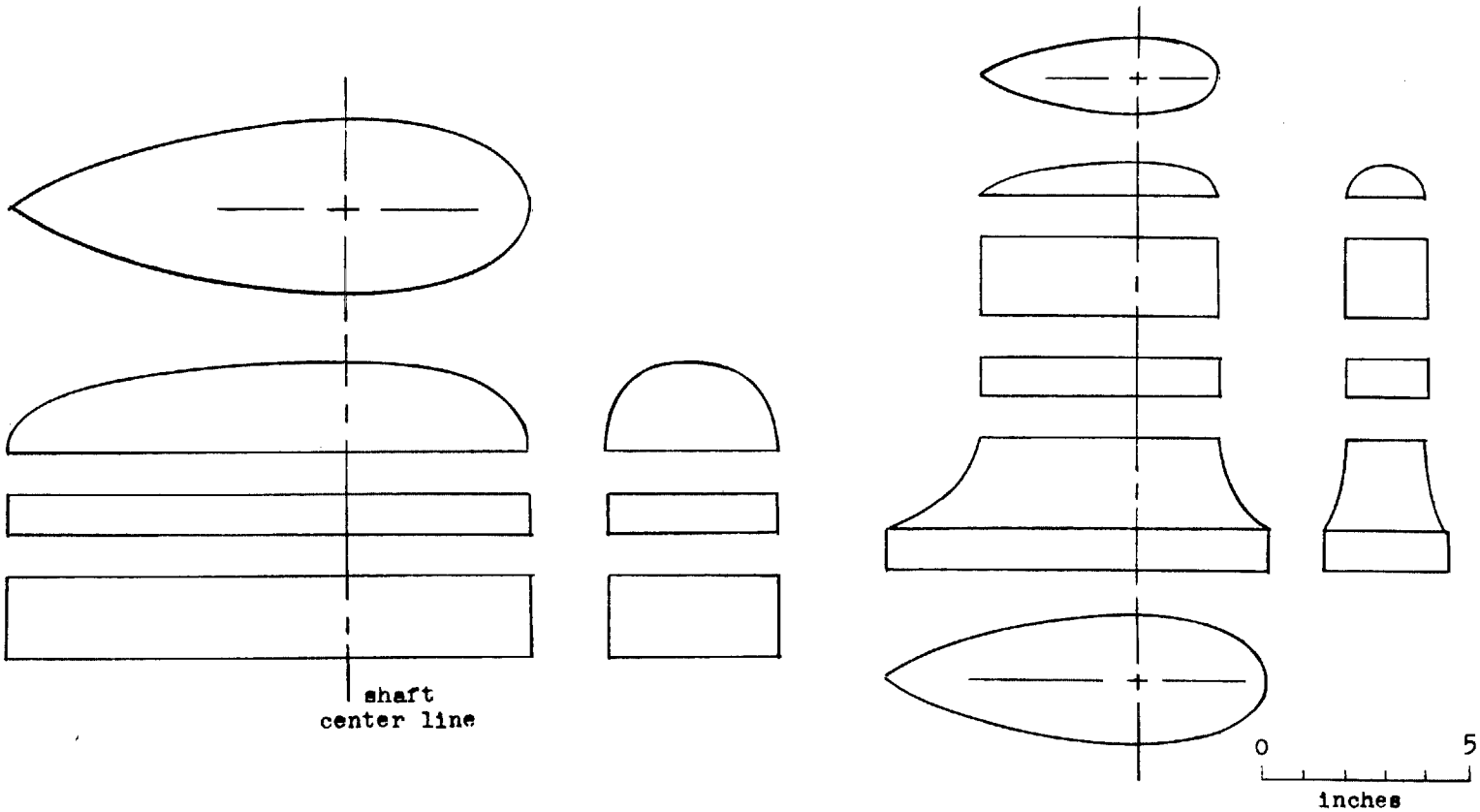

(a) Wide pylon components.

(b) Narrow pylon components.

Figure 5.- Conventional pylon tops and spacer segments.

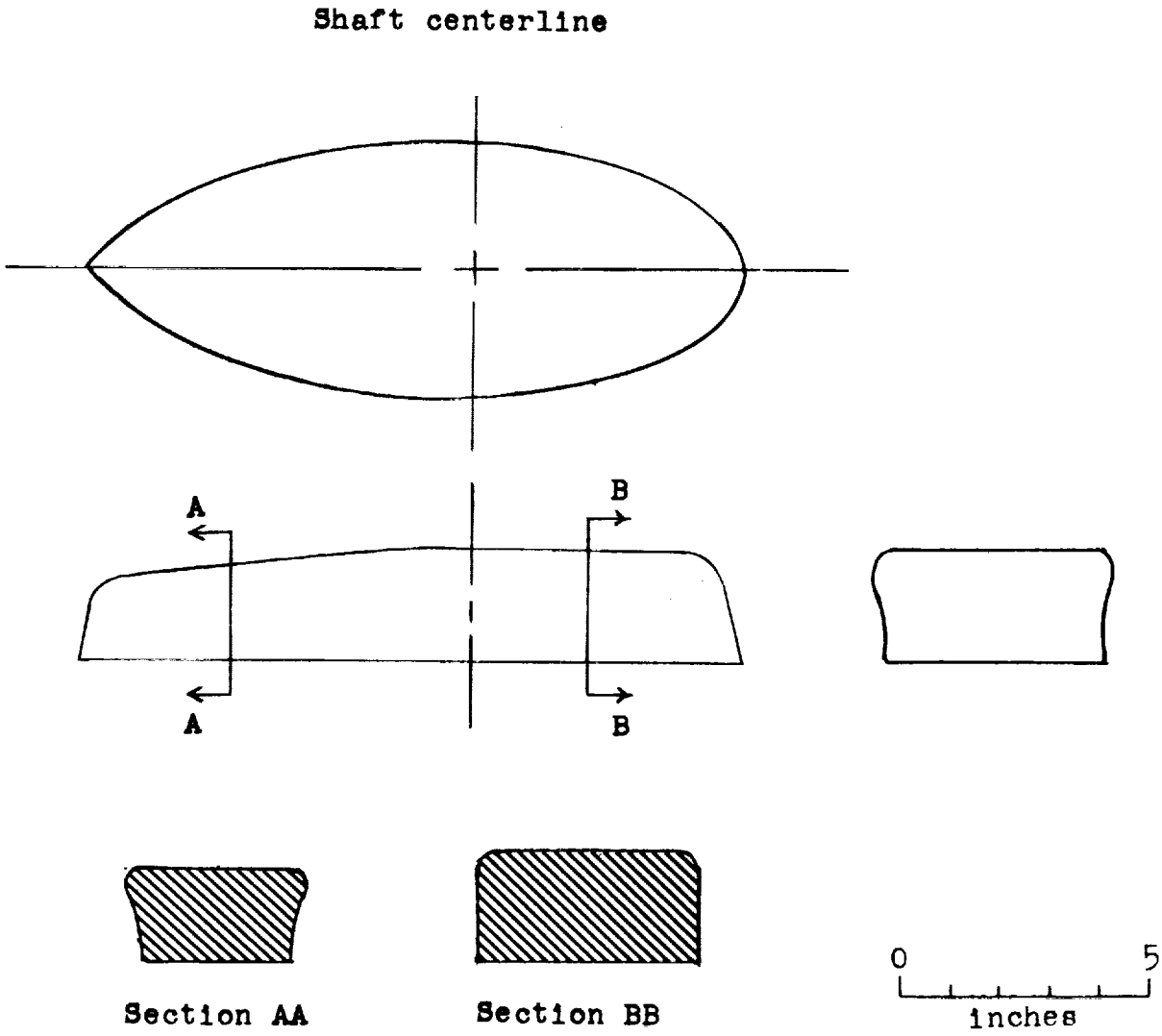

Figure 6.- Ramp top for wide pylon.

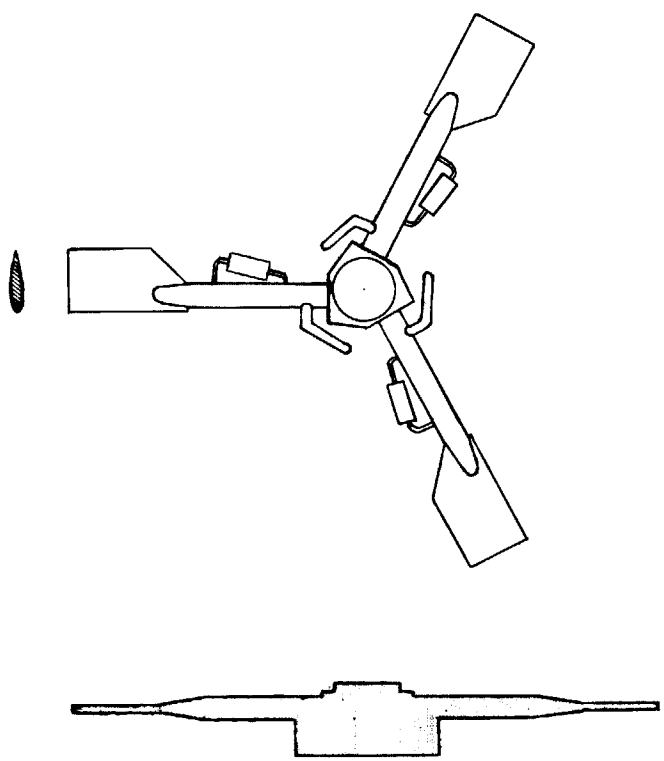

Projected view

(a) Conventional.

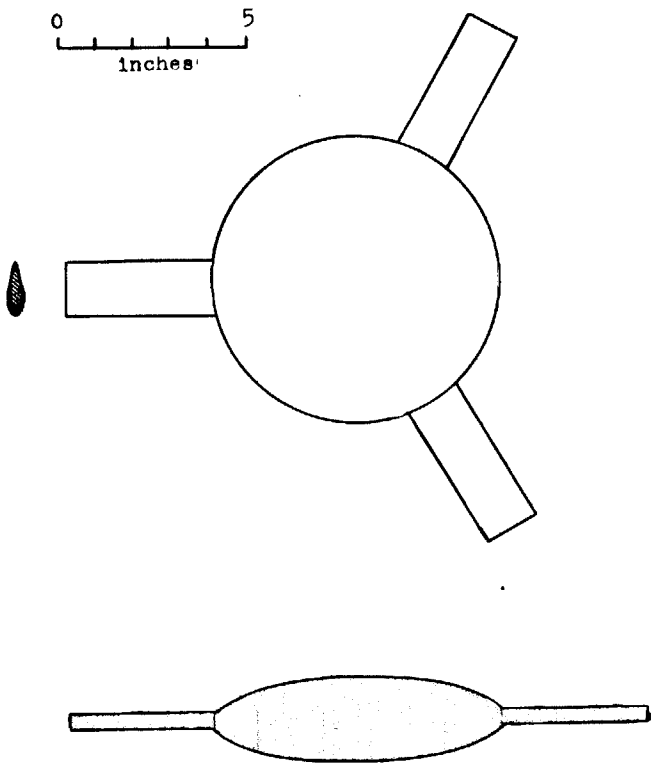

Projected view

(b) Streamlined.

Figure 7.- Rotor hubs.

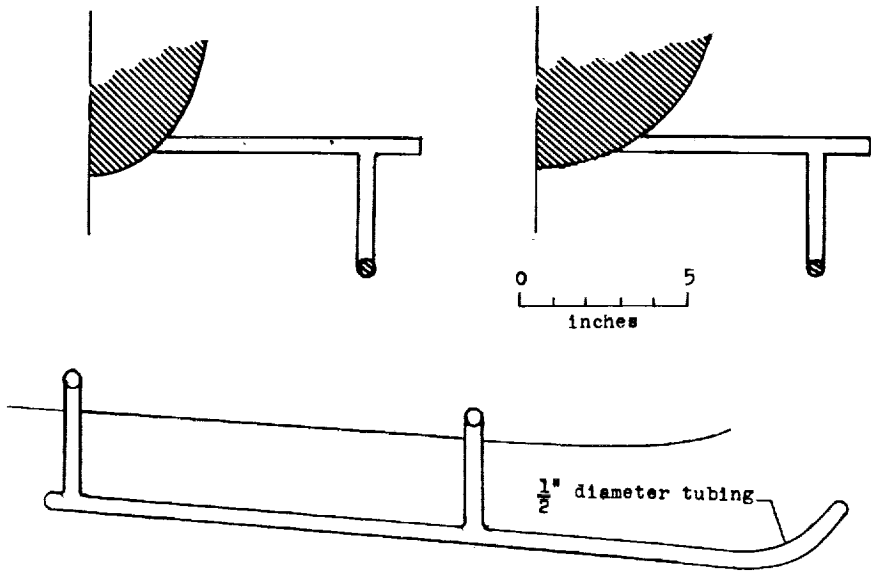

(a) Tubular.

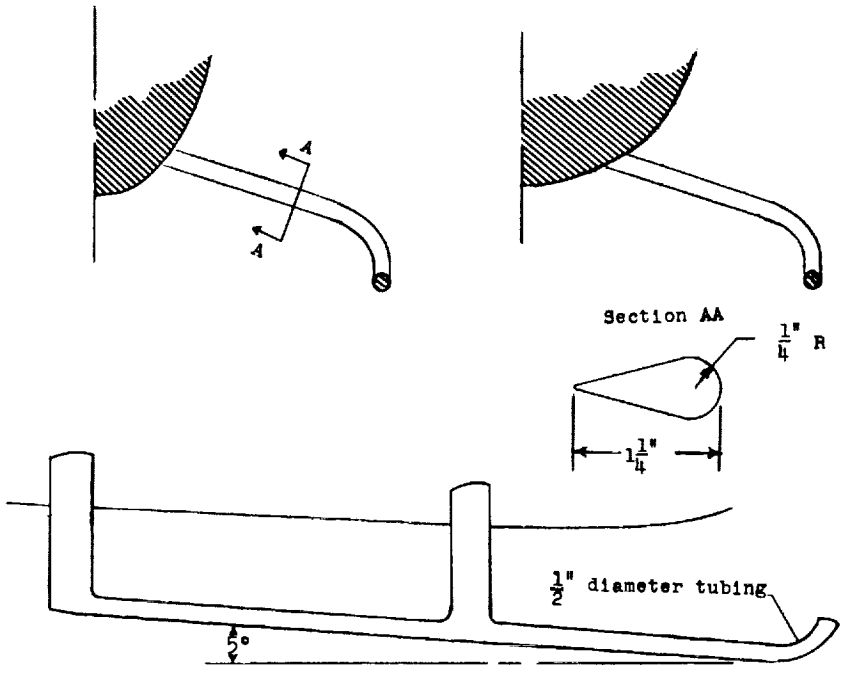

(b) Faired.

Figure 8.- Landing skids.

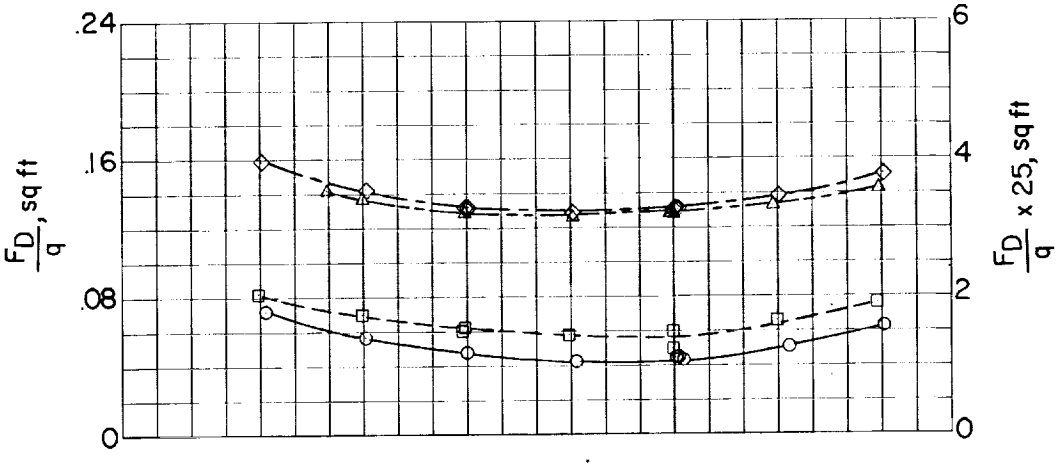

(a) Drag.

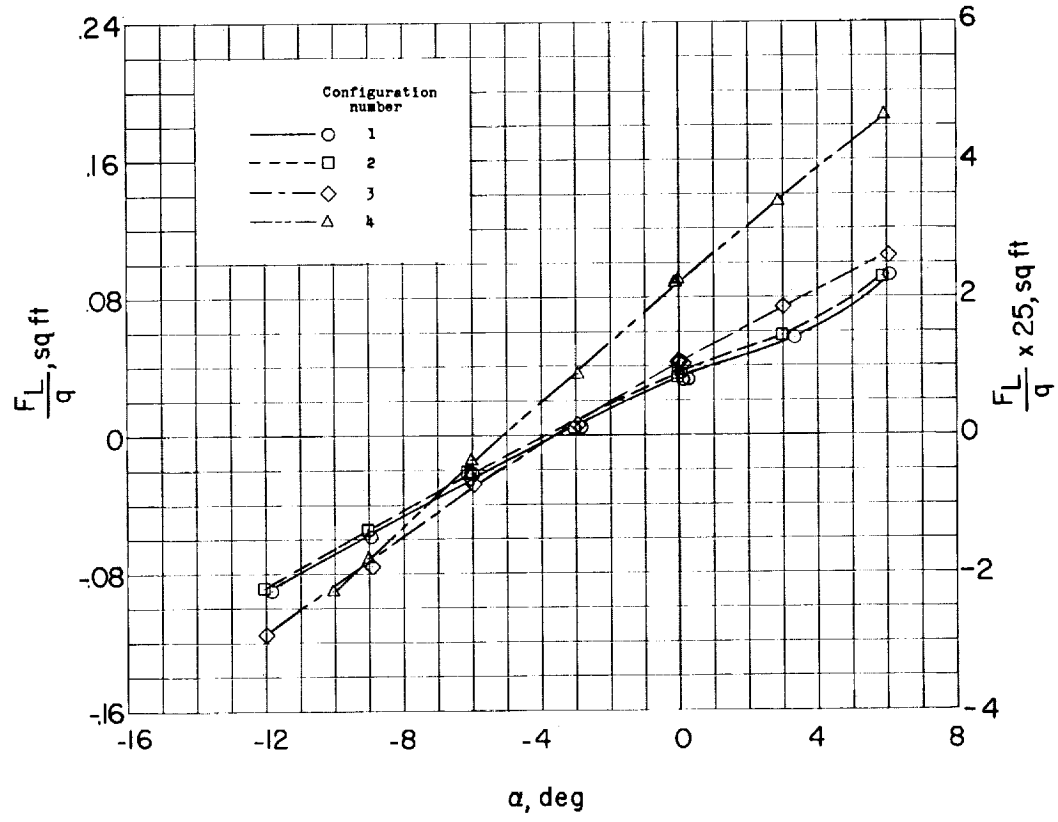

(b) Lift.

Figure 9.- Variation of lift and drag with angle of attack for the model A configurations listed in table II.

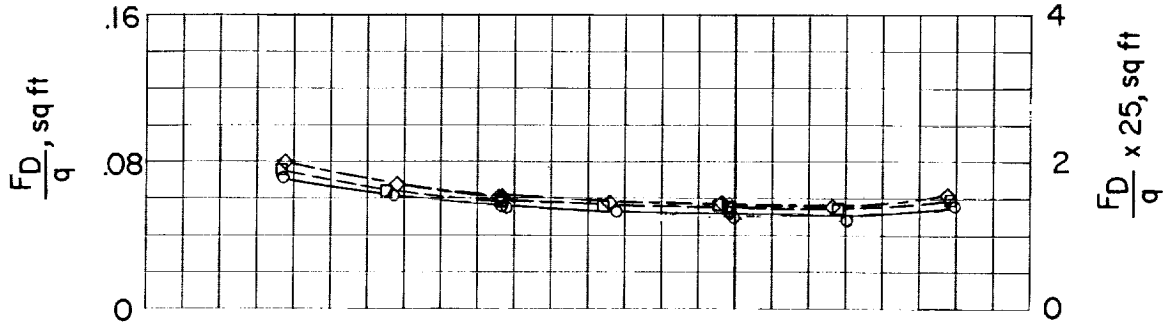

(a) Drag.

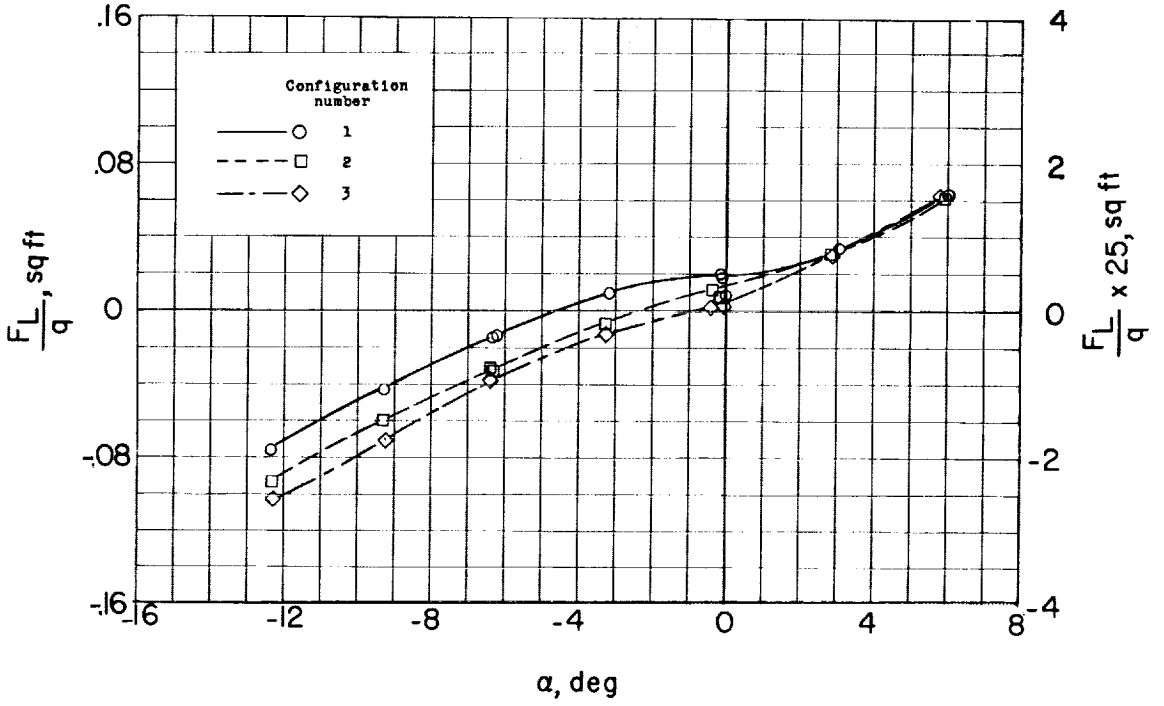

(b) Lift.

Figure 10.- Variation of lift and drag with angle of attack for the model B configurations listed in table II.

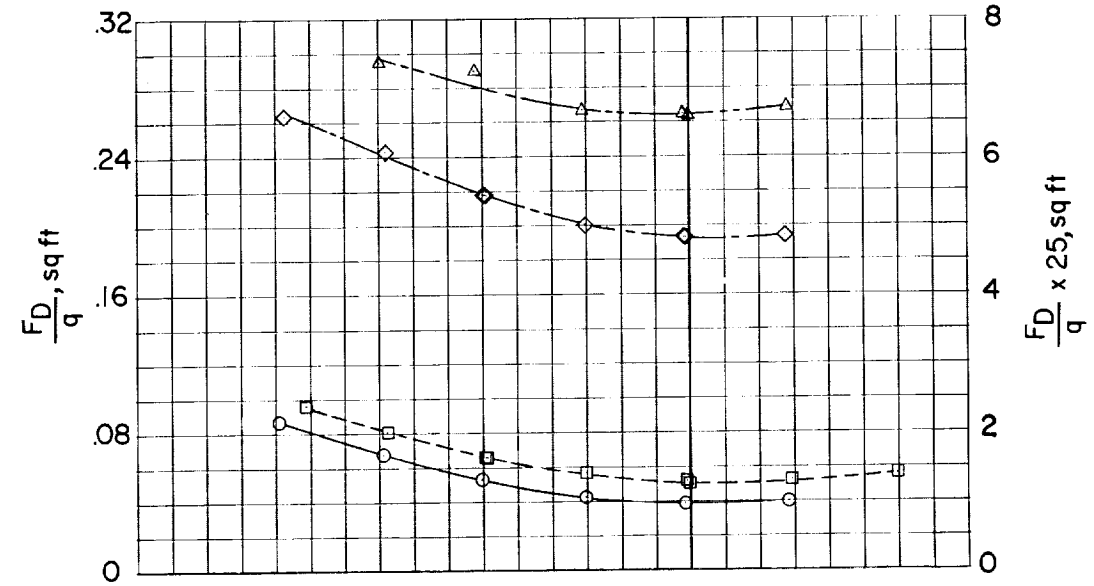

(a) Drag.

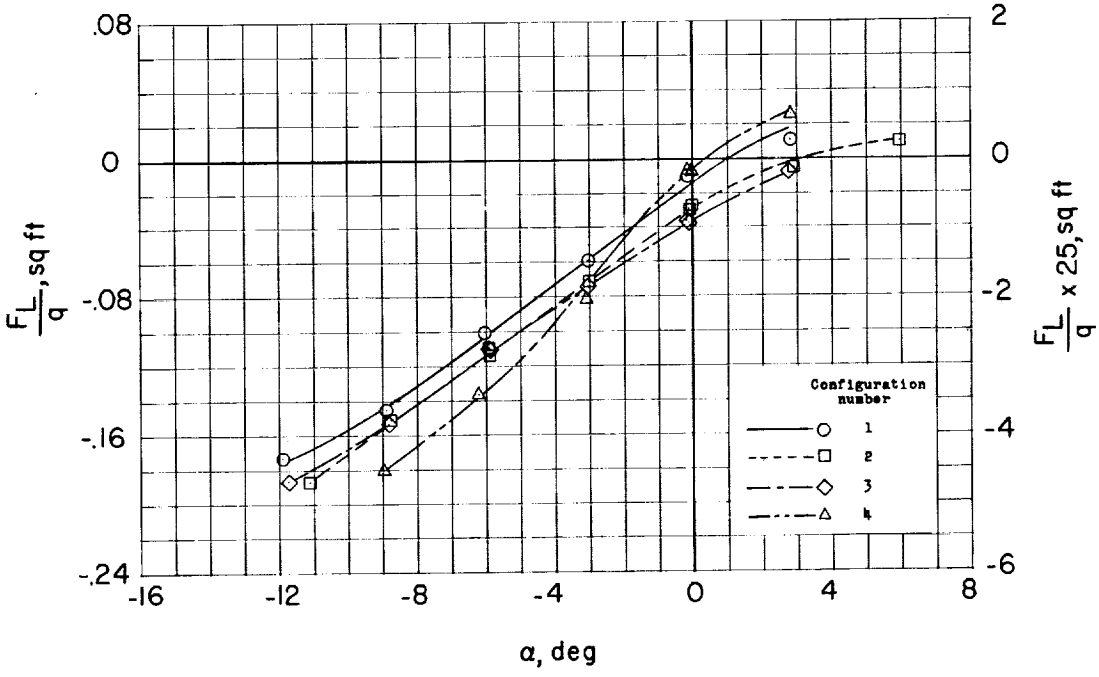

(b) Lift.

Figure 11.- Variation of lift and drag with angle of attack for the model C configurations listed in table II.

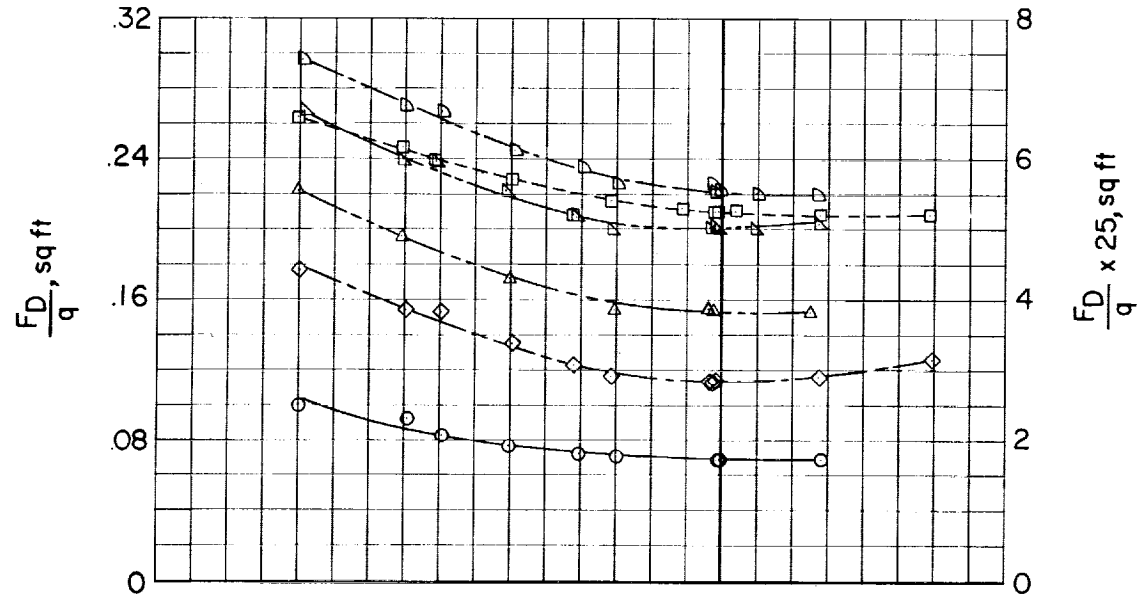

(a) Drag.

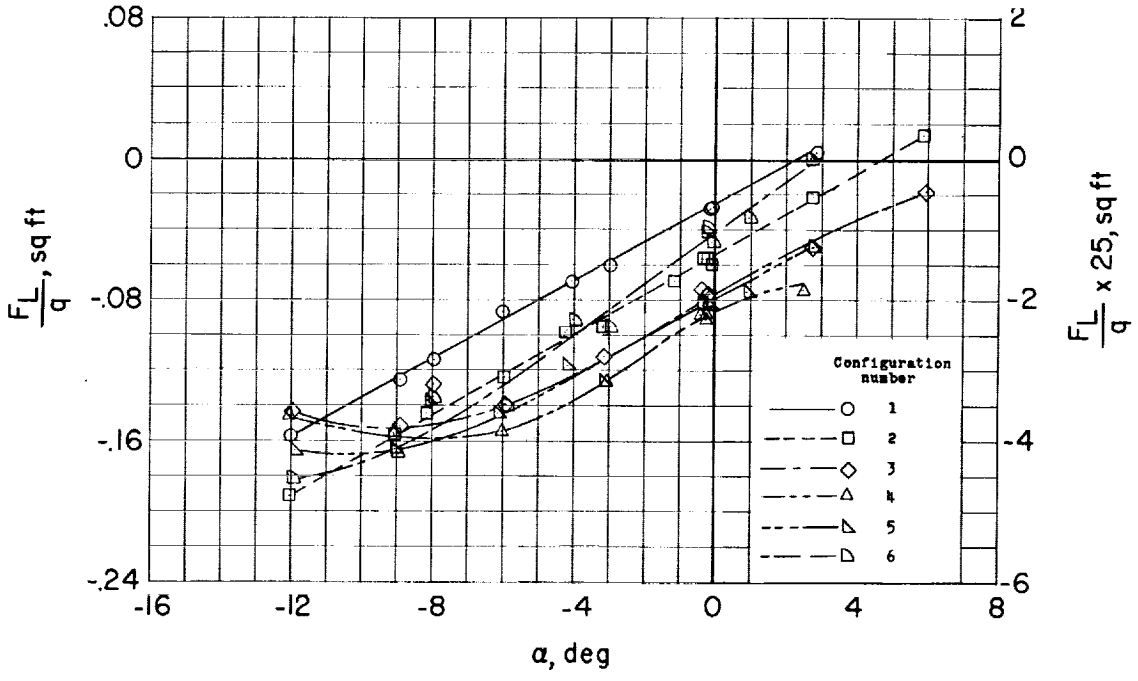

(b) Lift.

Figure 12.- Variation of lift and drag with angle of attack for the model D configurations listed in table II.

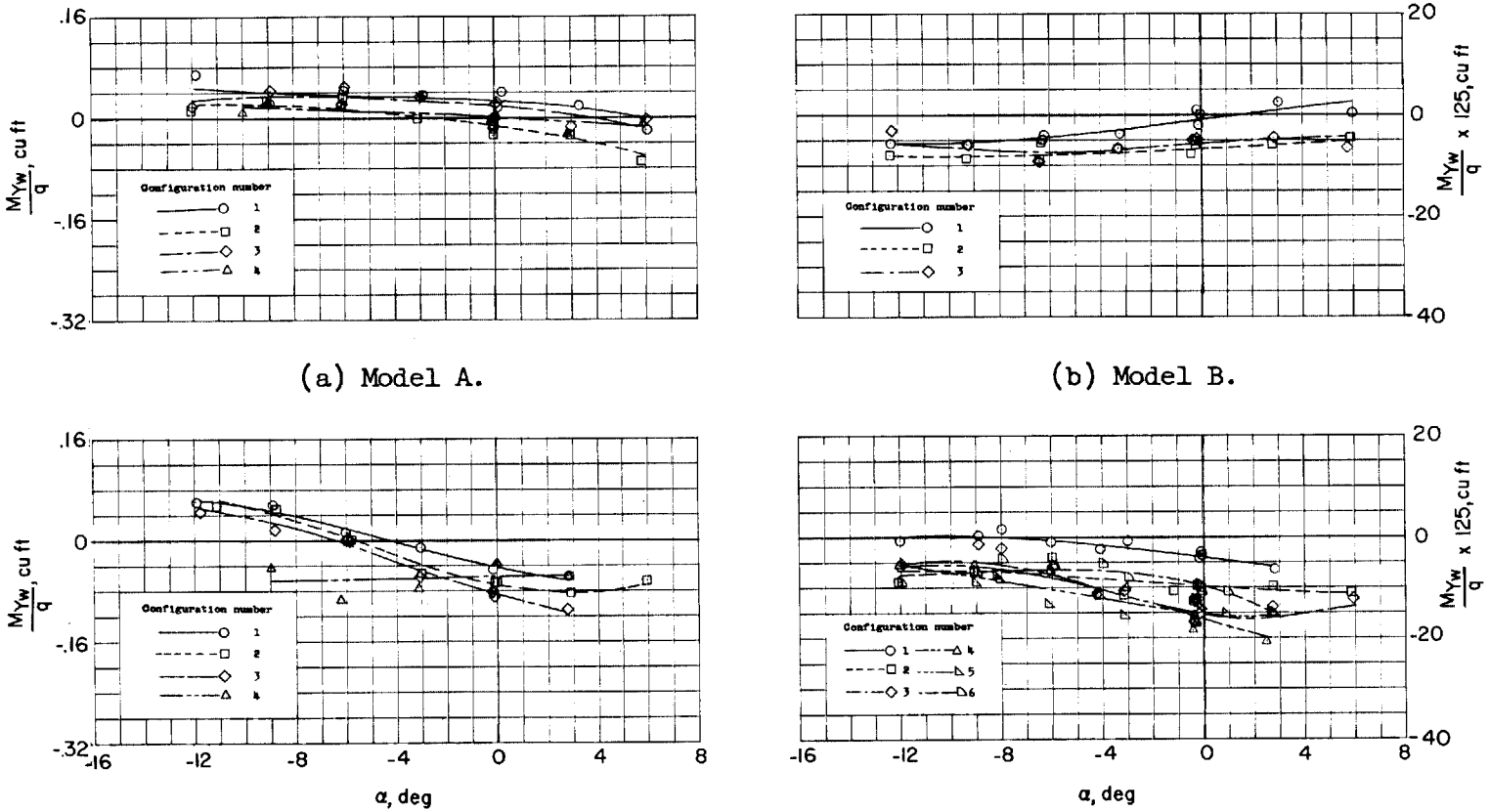

(a) Model A.

(b) Model B.

(c) Model C.

(d) Model D.

Figure 13.- Variation of pitching moment with angle of attack for all models.

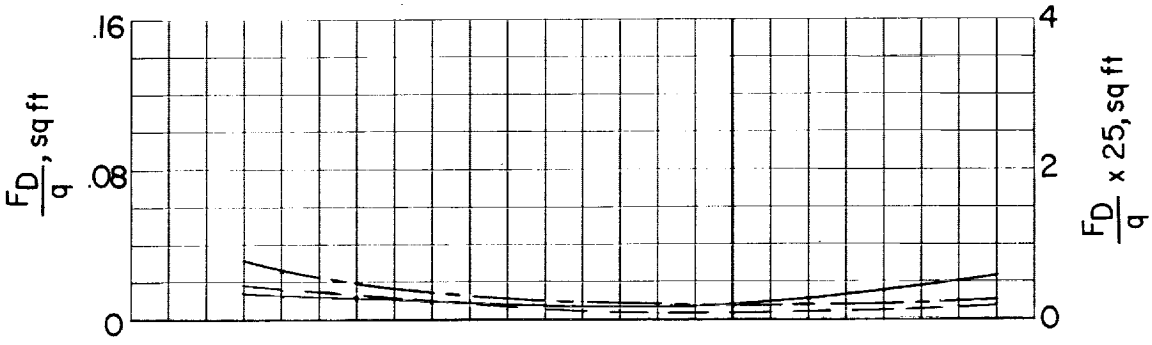

(a) Drag.

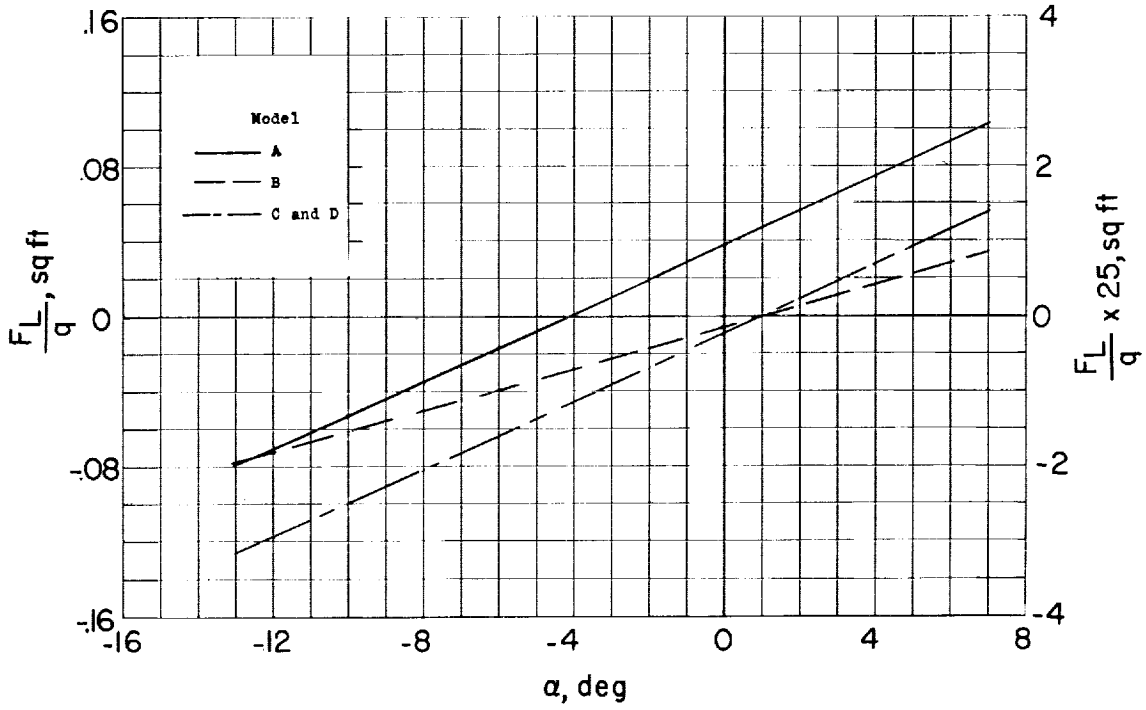

(b) Lift.

Figure 14.- Calculated lift and drag and pitching moment for the horizontal trim surfaces of the test models. Calculations include correction for tunnel stream angle.

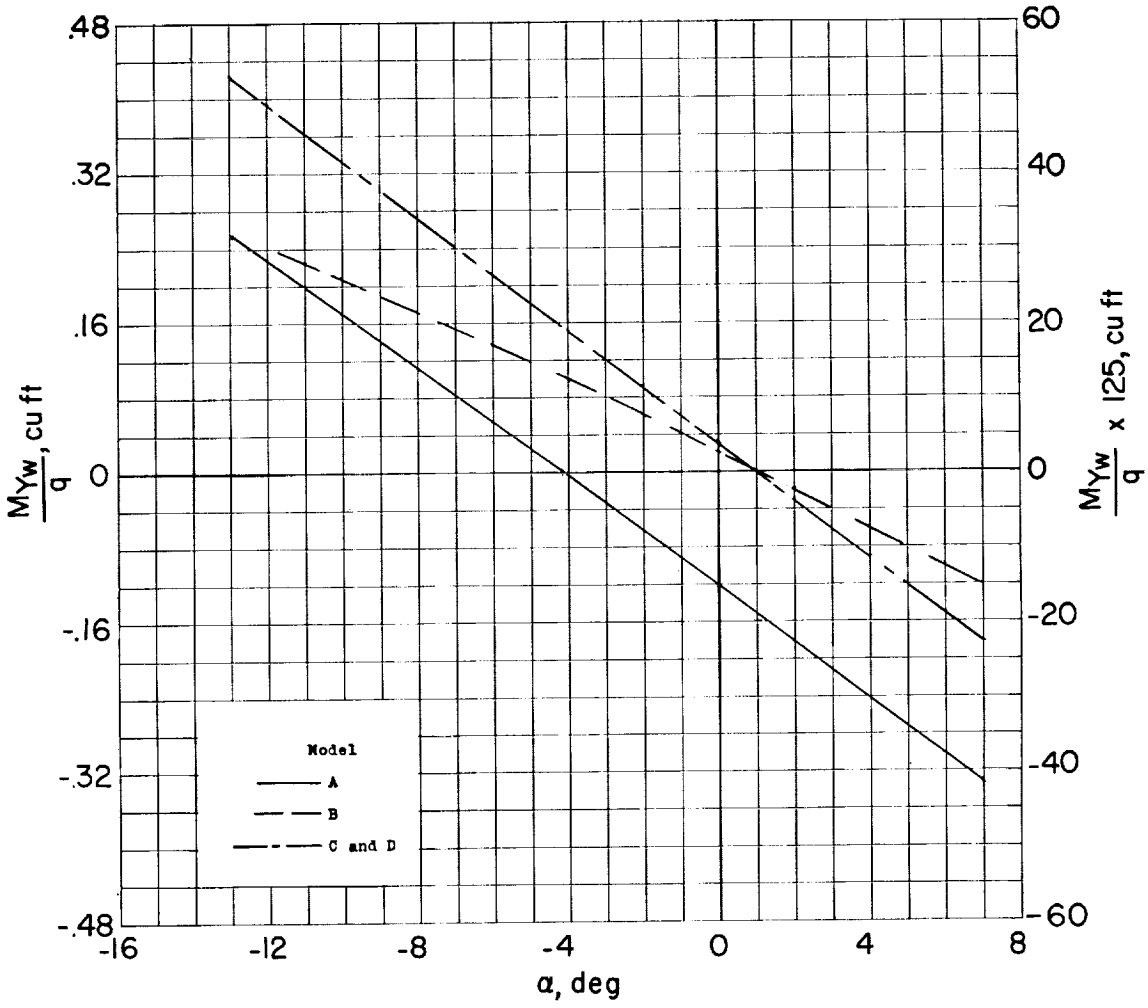

(c) Pitching moment.

Figure 14.- Concluded.

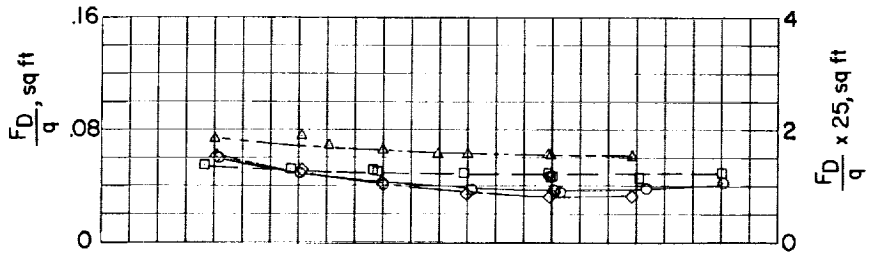

(a) Drag.

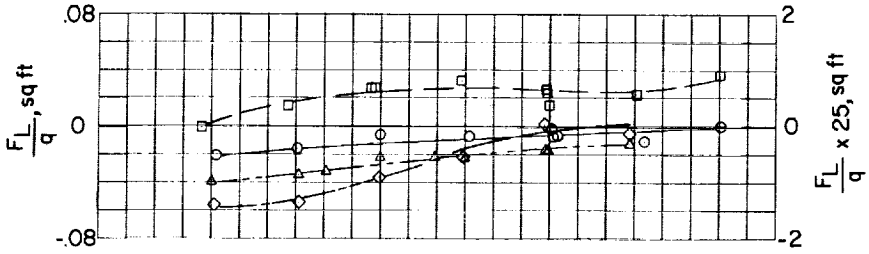

(b) Lift.

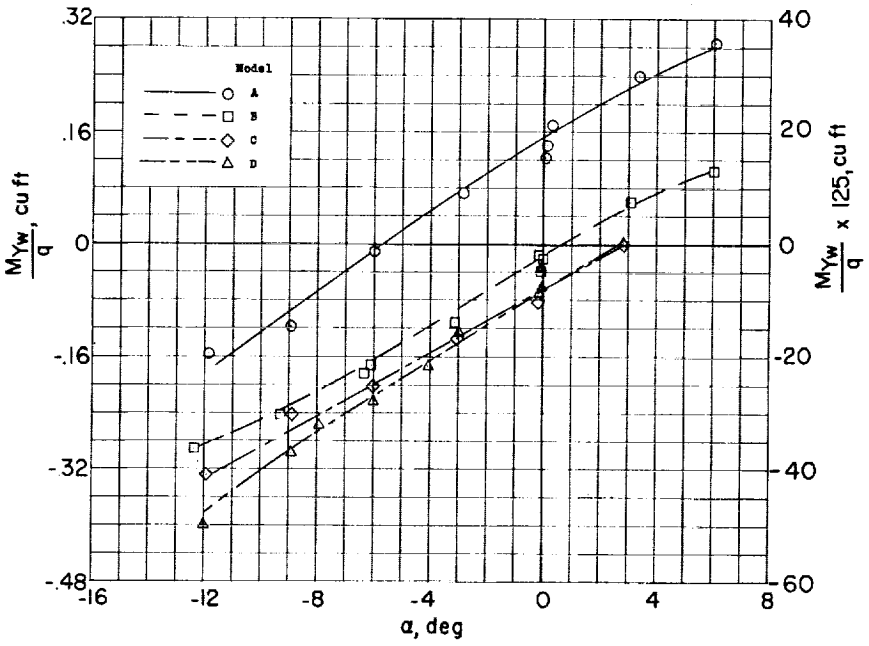

(c) Pitching moment.

Figure 15.- A comparison of the characteristics of the basic fuselage shapes. Calculated horizontal-tail aerodynamics subtracted.

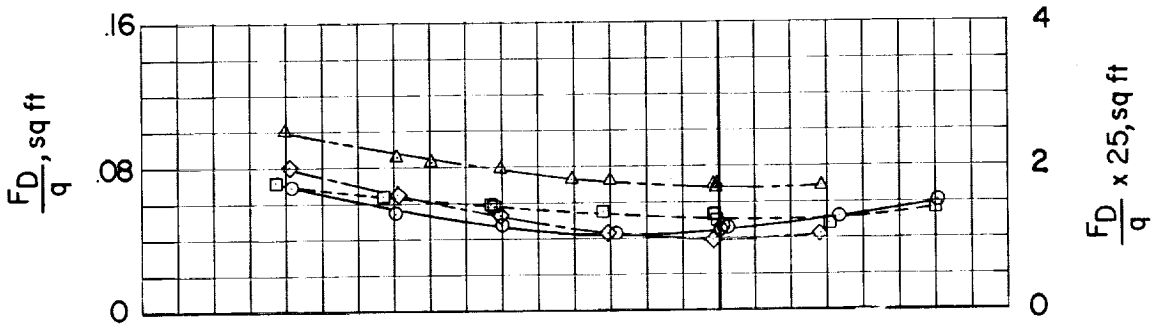

(a) Drag.

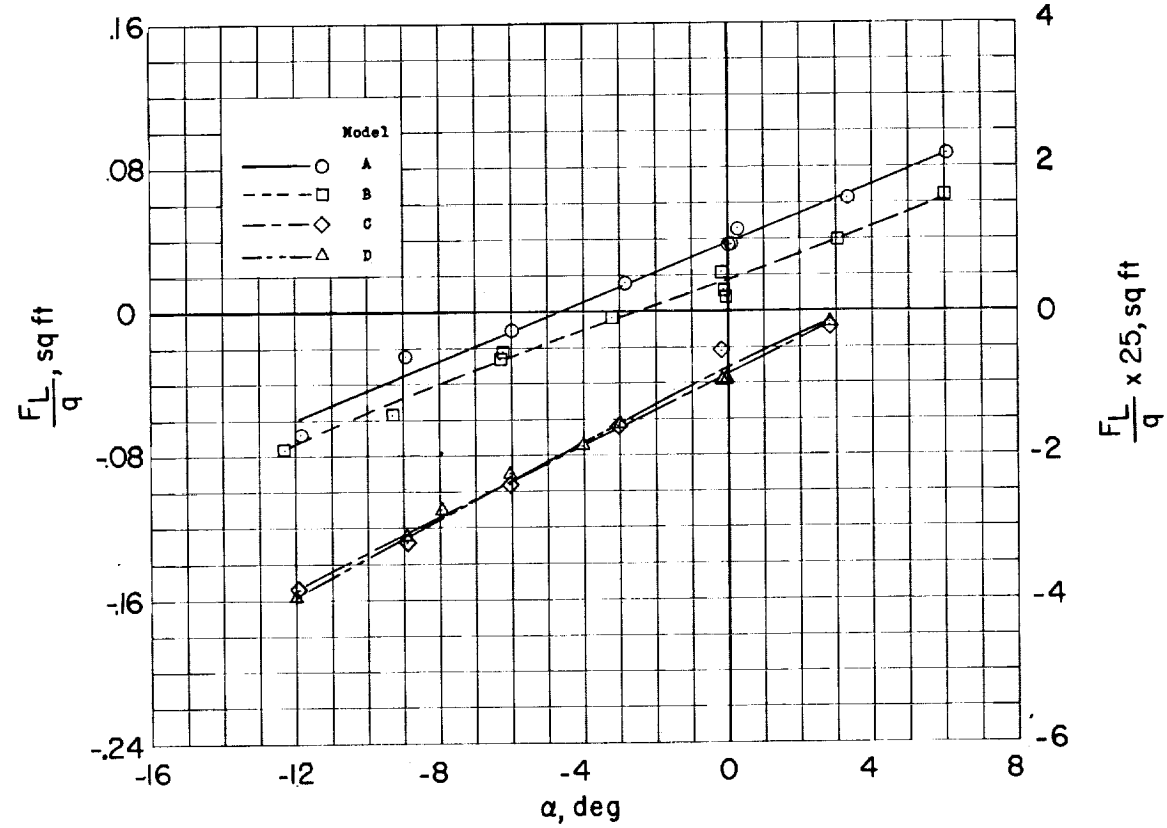

(b) Lift.

Figure 16.- Basic fuselage shapes with horizontal-tail surface. Fuselage pitching moment trimmed to zero.

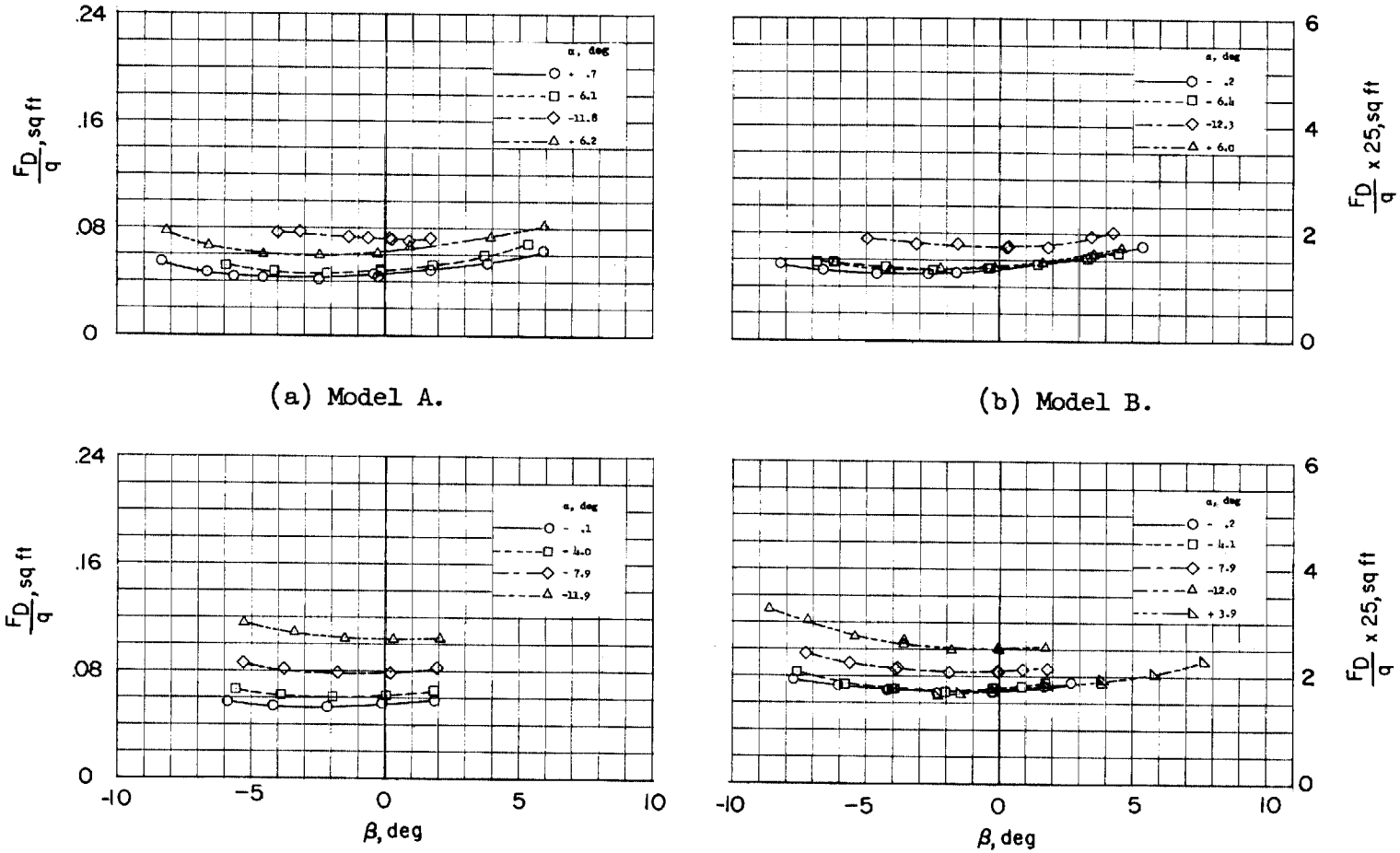

(a) Model A.

(b) Model B.

(c) Model C.

(d) Model D.

Figure 17.- Variation of drag with sideslip at several angles of attack for fuselage shapes.

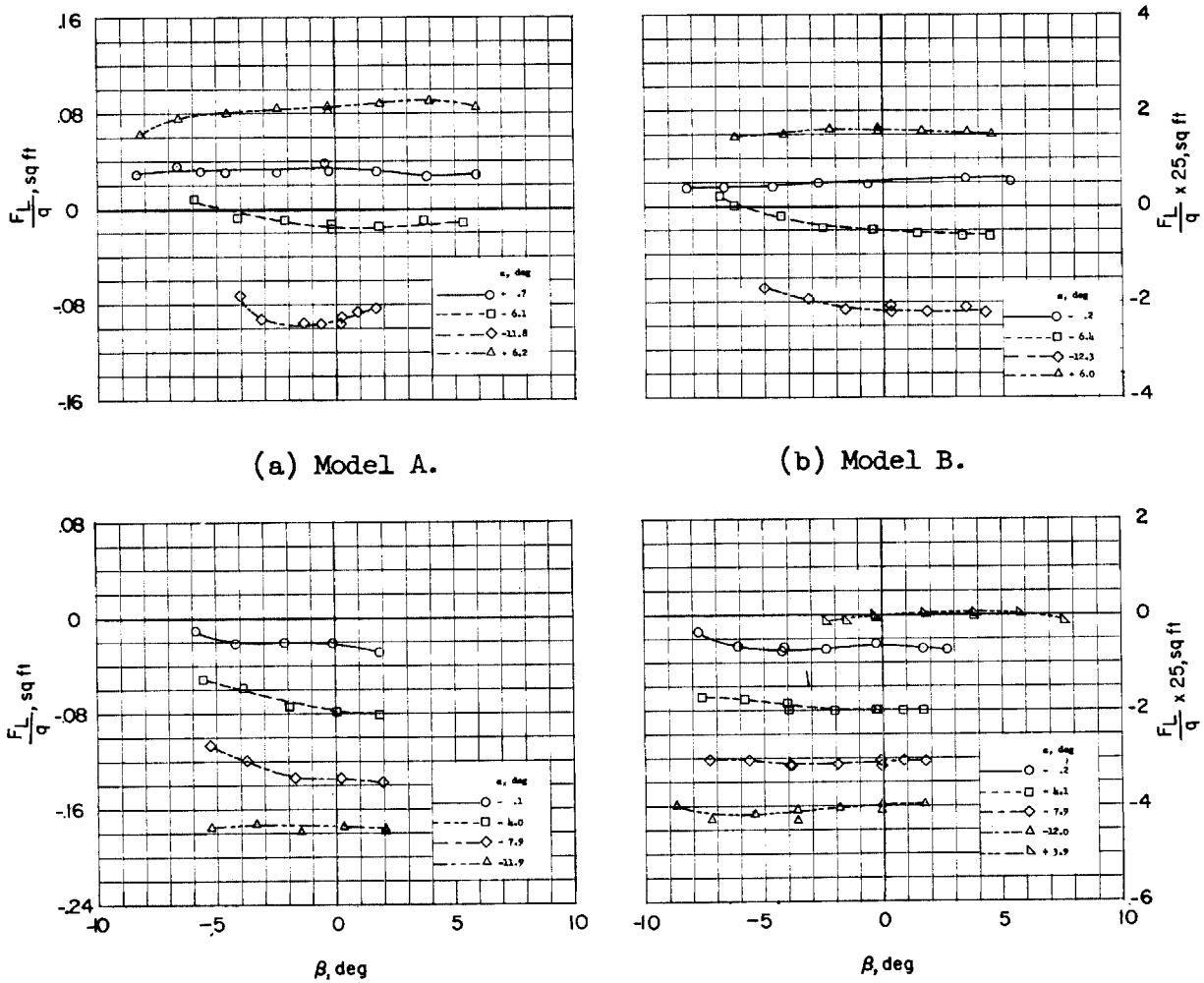

(a) Model A.

(b) Model B.

(c) Model C.

(d) Model D.

Figure 18.- Variation of lift with sideslip at several angles of attack for fuselage shapes.

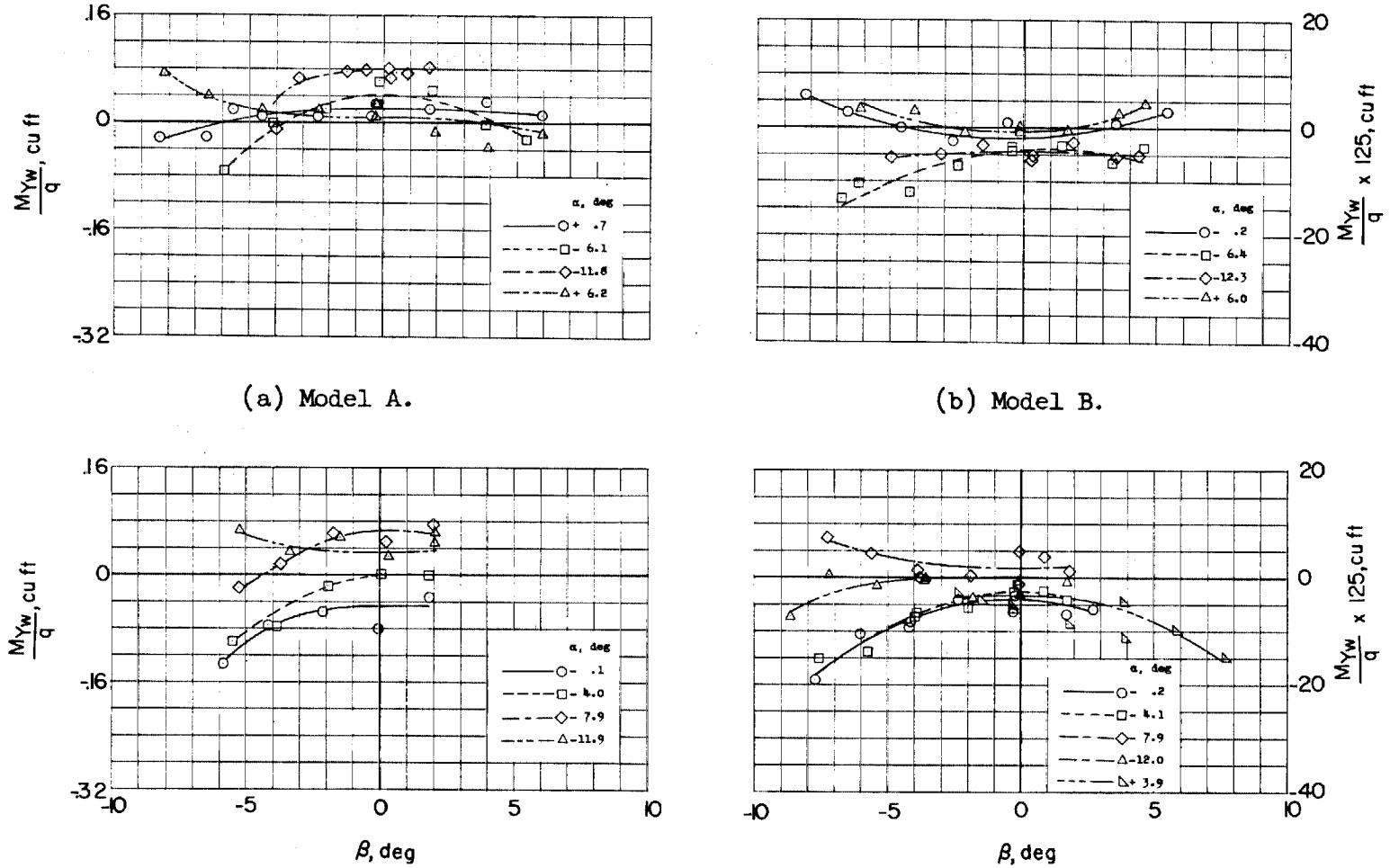

(a) Model A.

(b) Model B.

(c) Model C.

(d) Model D.

Figure 19.- Variation of pitching moment with sideslip at several angles of attack for fuselage shapes.

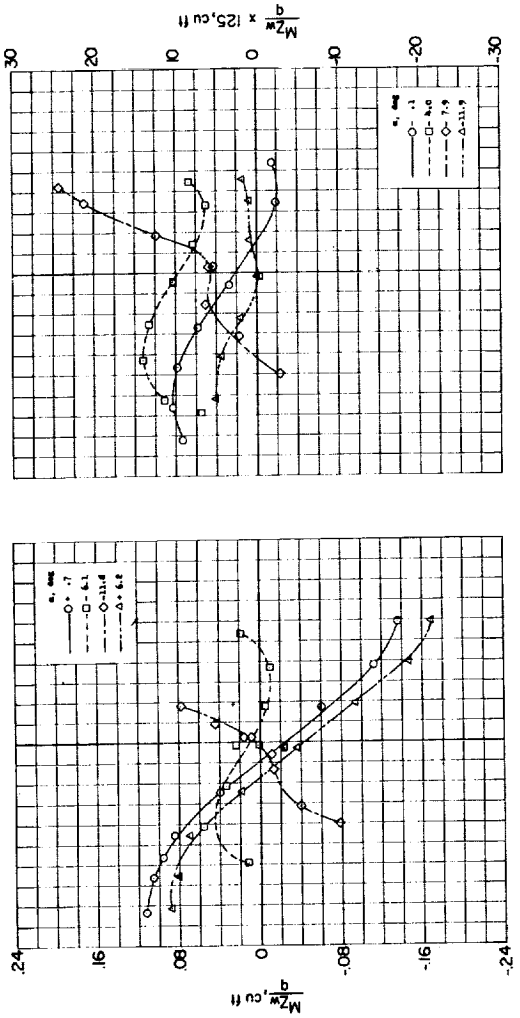

(a) Model A.

(b) Model B.

(c) Model C.

(d) Model D.

Figure 20.- Variation of yawing moment with sideslip at several angles of attack for fuselage shapes.

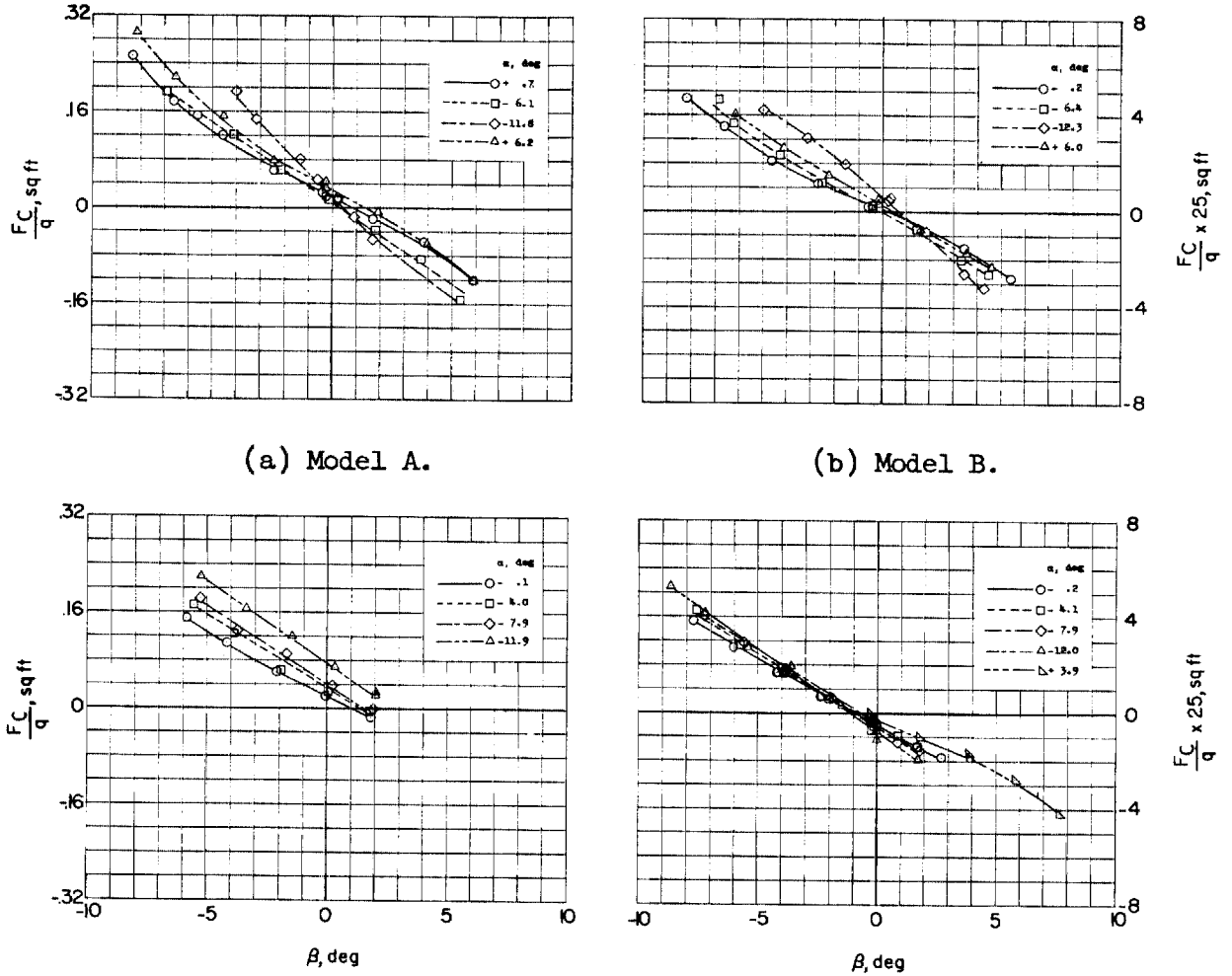

(a) Model A.

(b) Model B.

(c) Model C.

(d) Model D.

Figure 21.- Variation of side force with sideslip at several angles of attack for fuselage shapes.

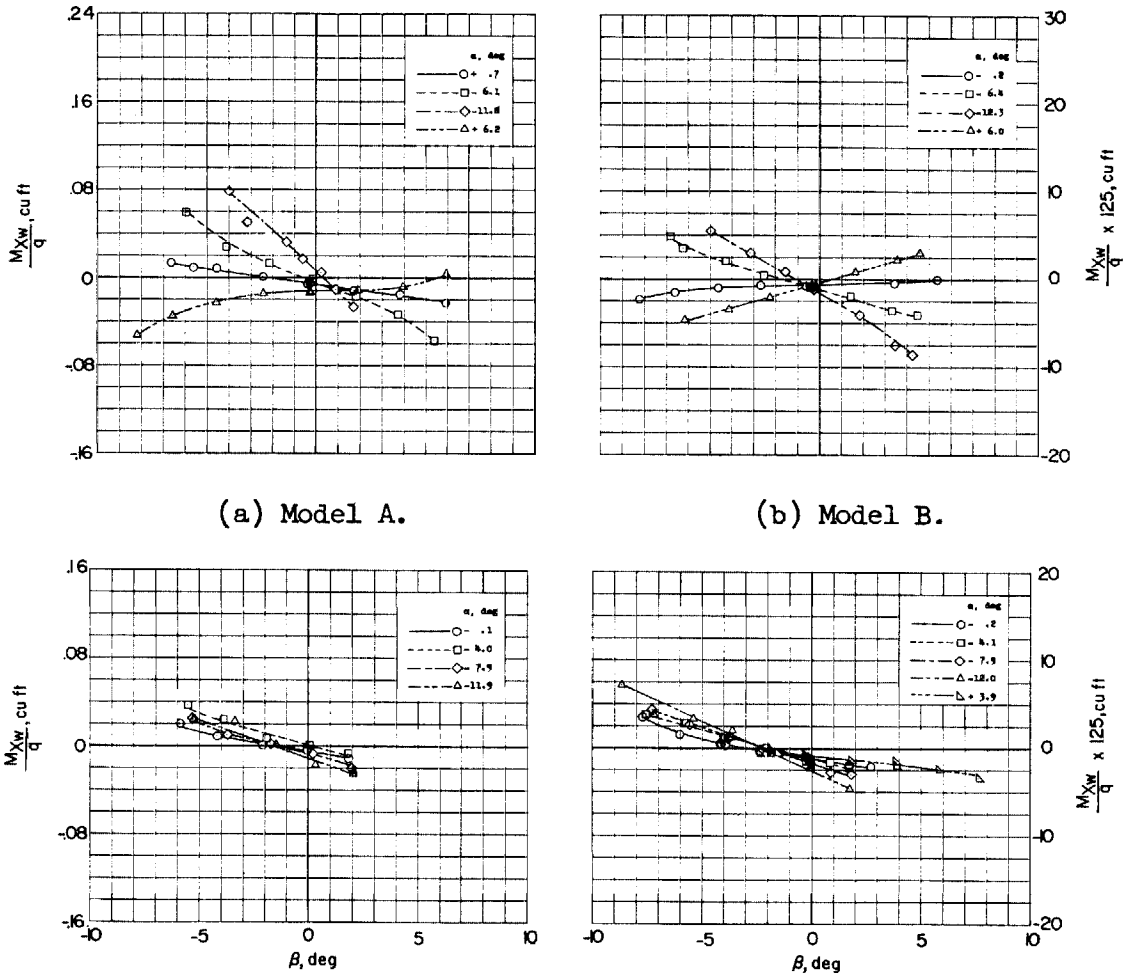

(a) Model A.

(b) Model B.

(c) Model C.

(d) Model D.

Figure 22.- Variation of rolling moment with sideslip at several angles of attack for fuselage shapes.

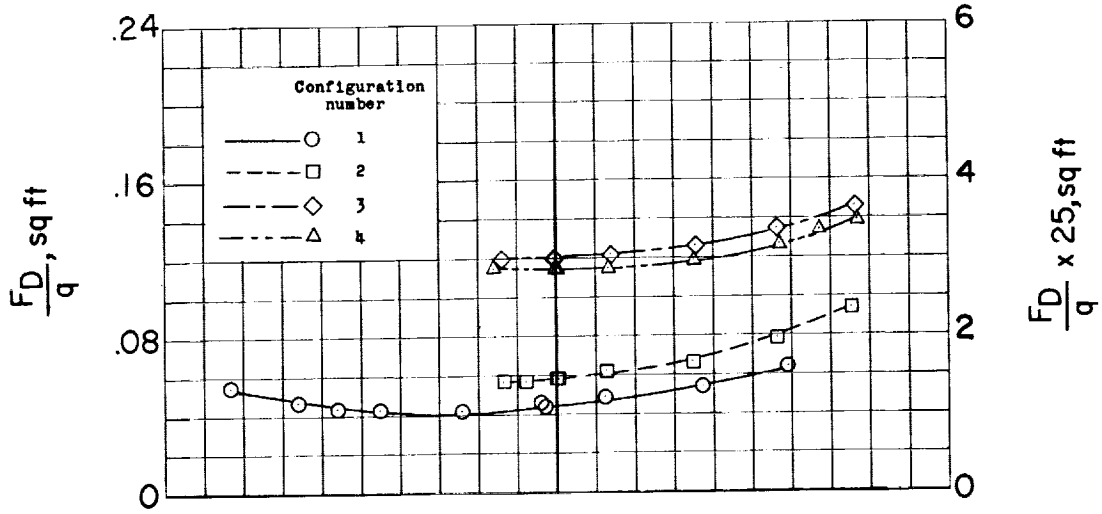

(a) Model A.

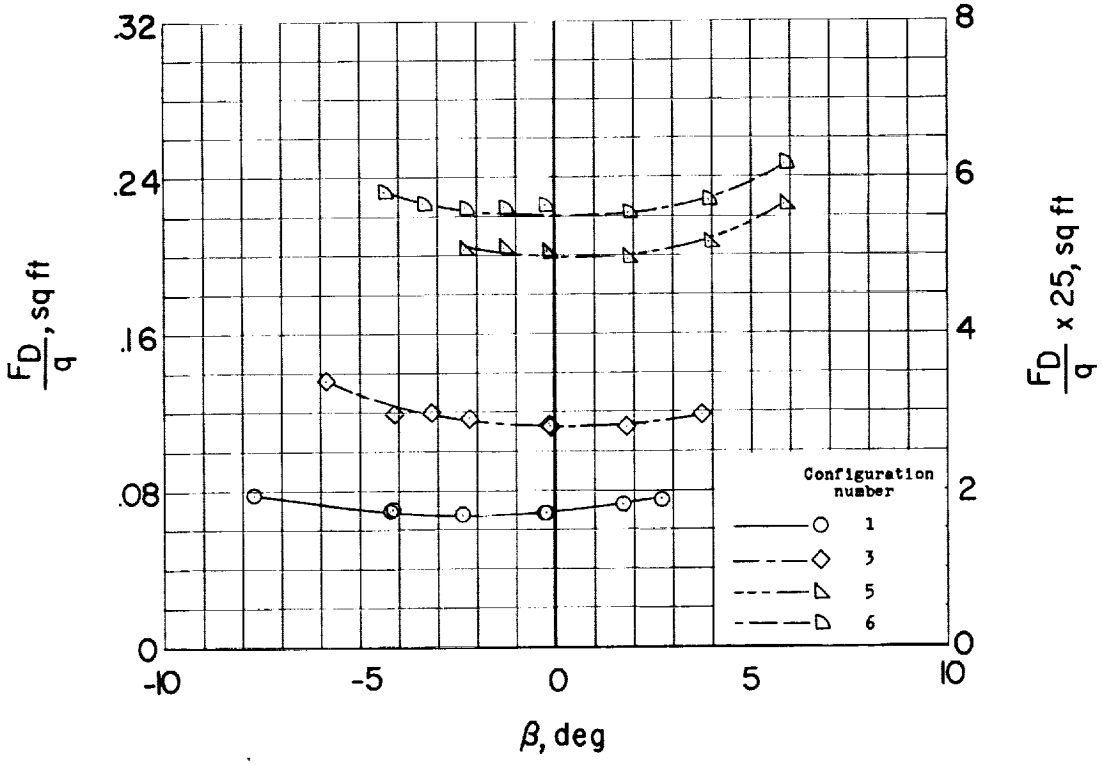

(b) Model D.

Figure 23.- Variation of parasite drag of models A and D with and without appendages $\alpha = 0^\circ$.

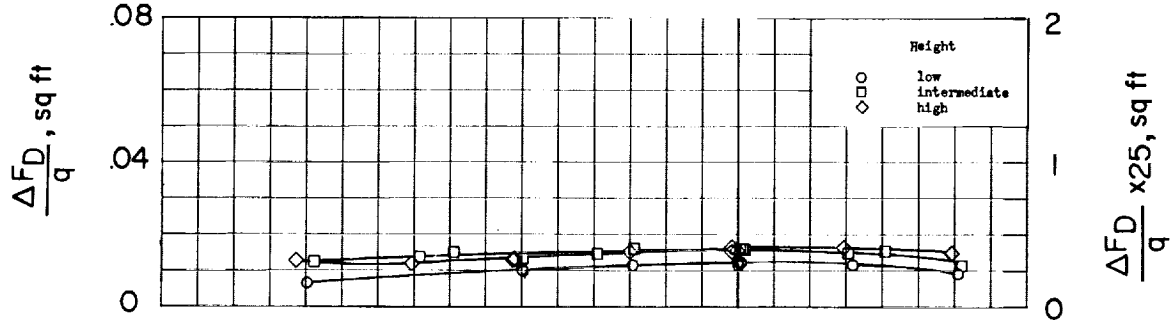

(a) Narrow pylon.

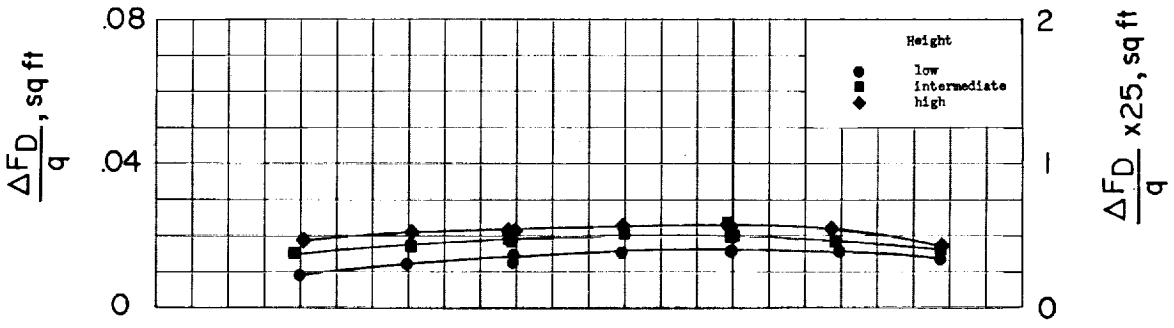

(b) Wide pylon.

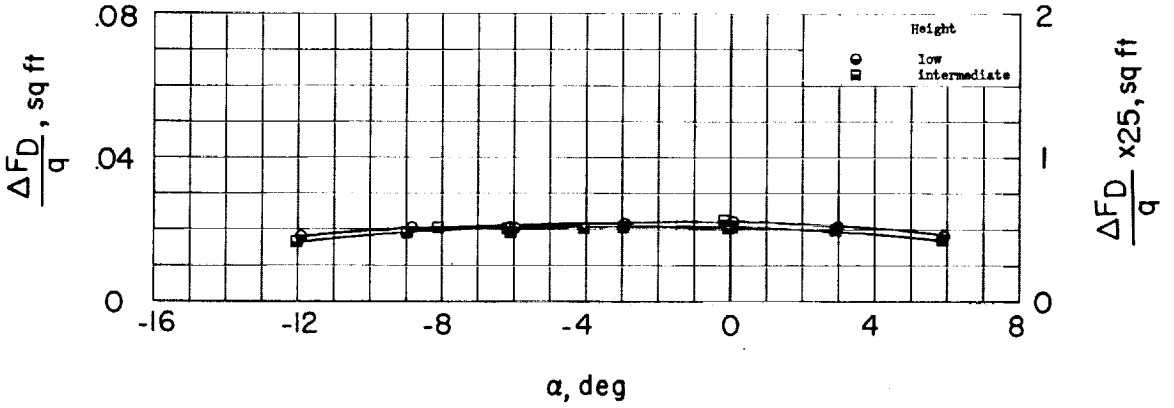

(c) Ramp pylon.

Figure 24.- Incremental drag divided by dynamic pressure for various pylons and pylon-hub configurations tested on model A.

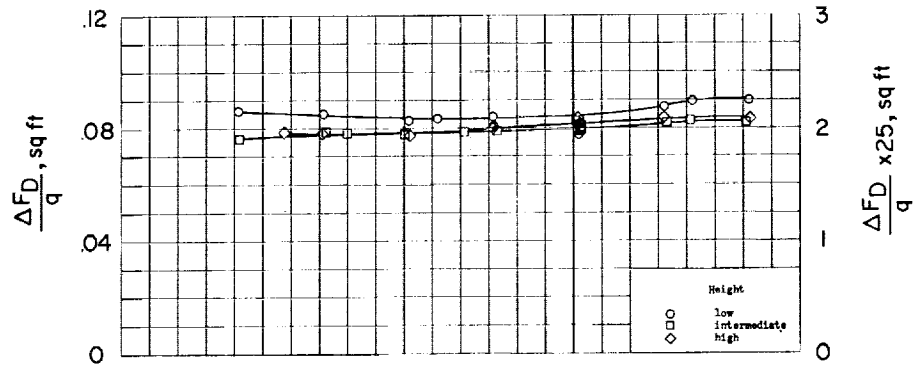

(d) Narrow pylon and conventional hub.

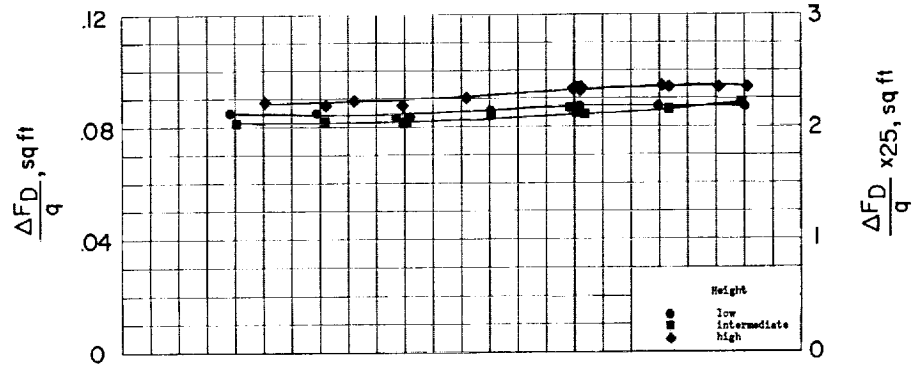

(e) Wide pylon and conventional hub.

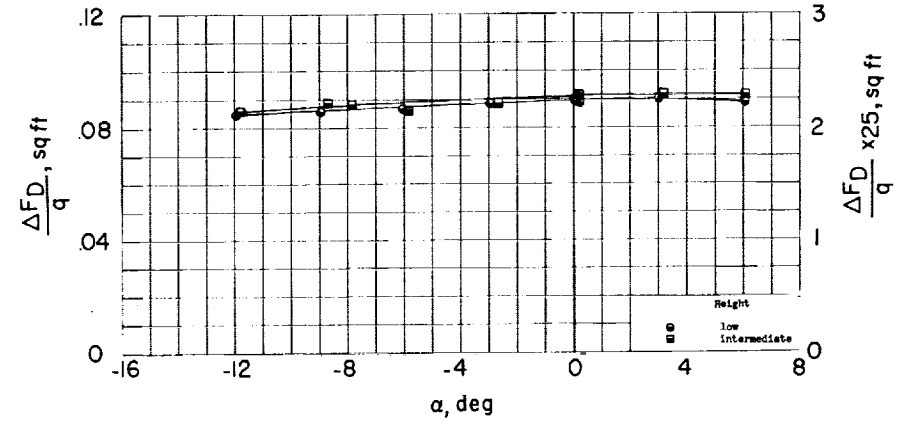

(f) Ramp pylon and conventional hub.

Figure 24.- Continued.

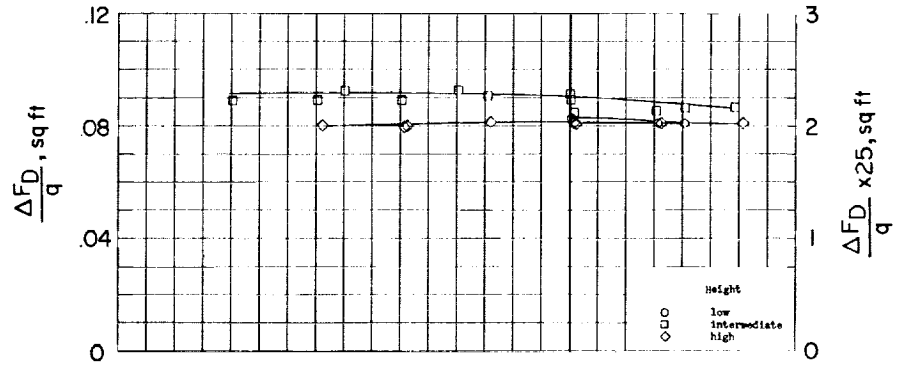

(g) Narrow pylon and faired hub.

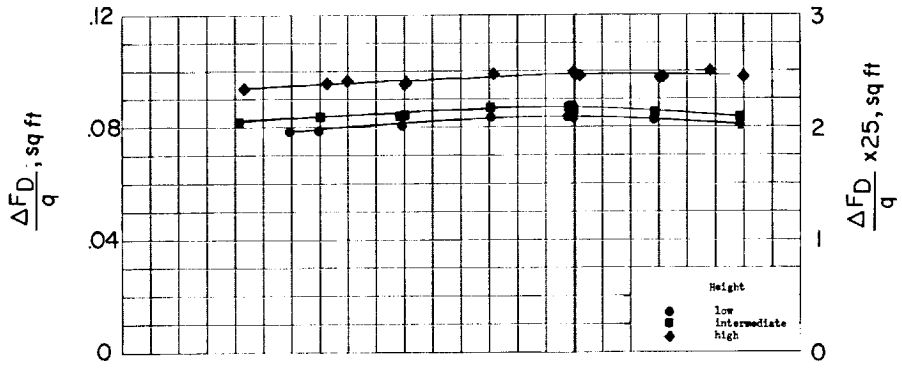

(h) Wide pylon and faired hub.

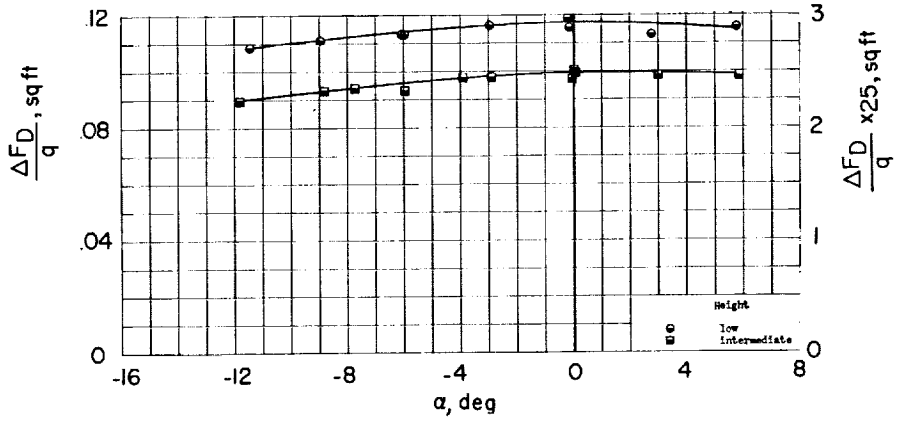

(i) Ramp pylon and faired hub.

Figure 24.- Concluded.

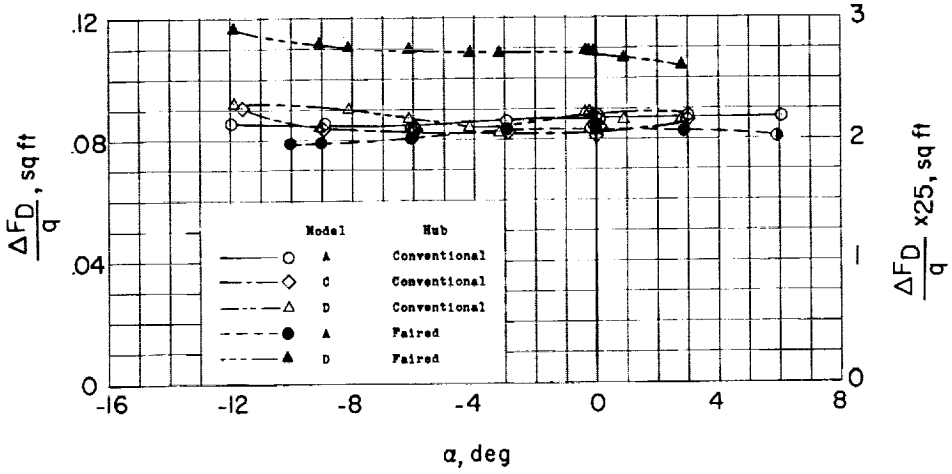

Figure 25.- Comparison of the incremental drag of two hub-pylon configurations when tested on several fuselage shapes. The wide pylon, low height was used in all cases.

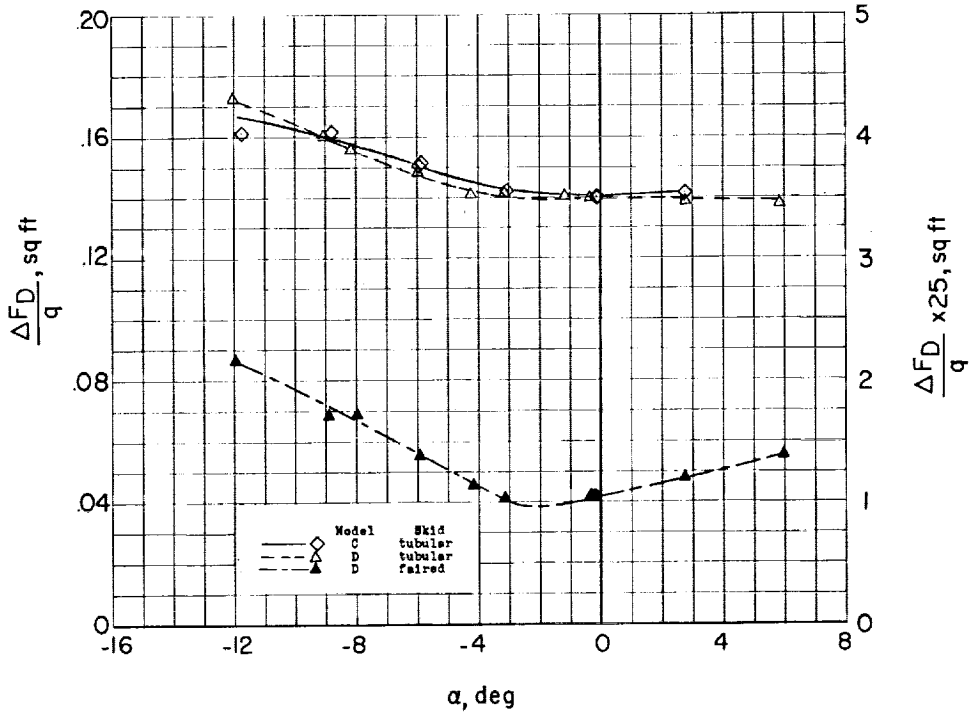

(a) Drag increment.

Figure 26.- Comparison of incremental aerodynamics of tubular and faired landing skids.

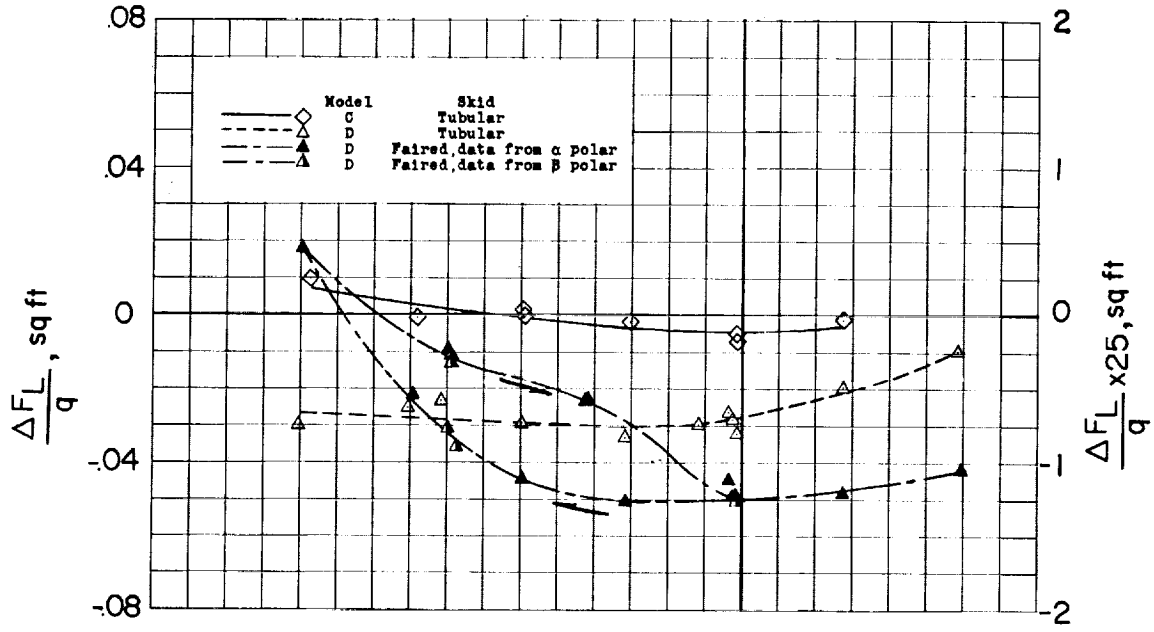

(b) Lift increment.

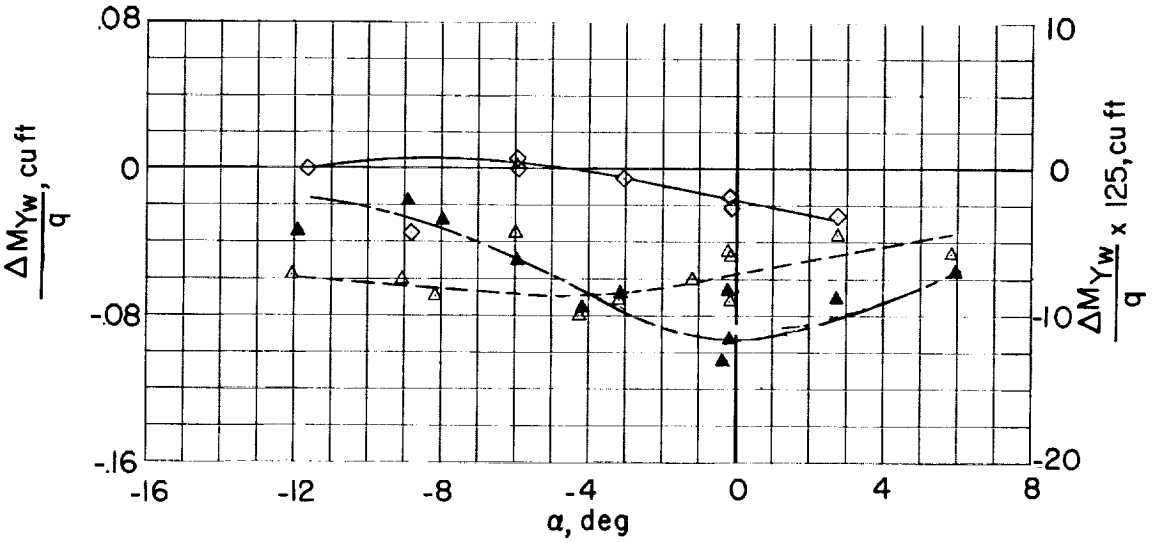

(c) Pitching-moment increment.

Figure 26.- Concluded.

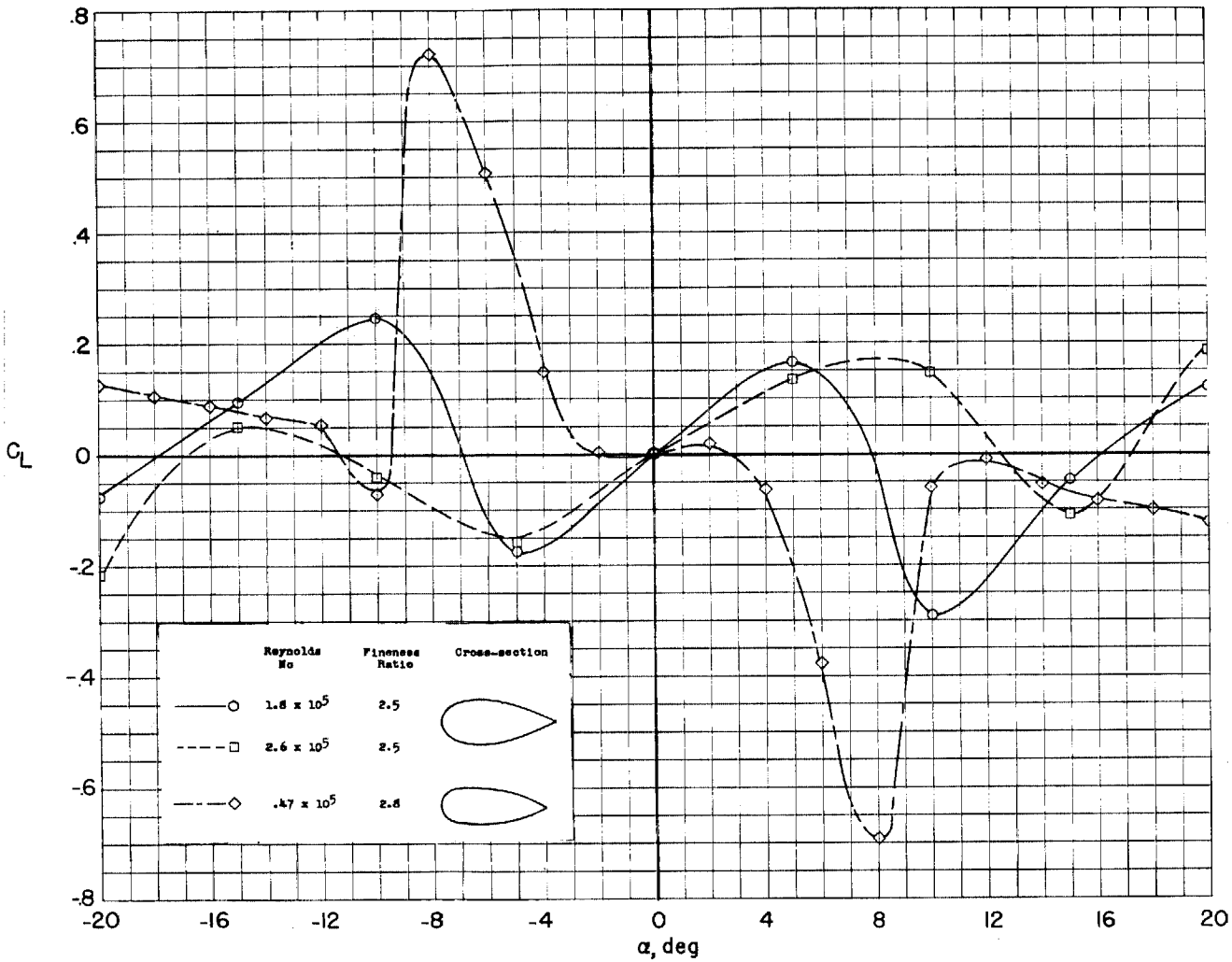

Figure 27.- Section lift coefficients for two strut shapes at low Reynolds number. (See refs. 27 and 28.)

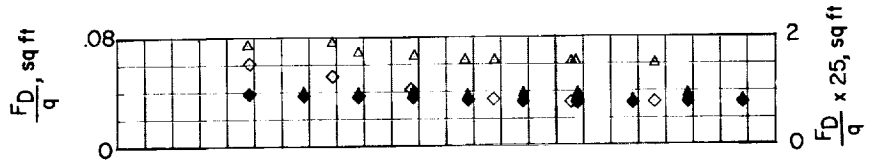

(a) Drag.

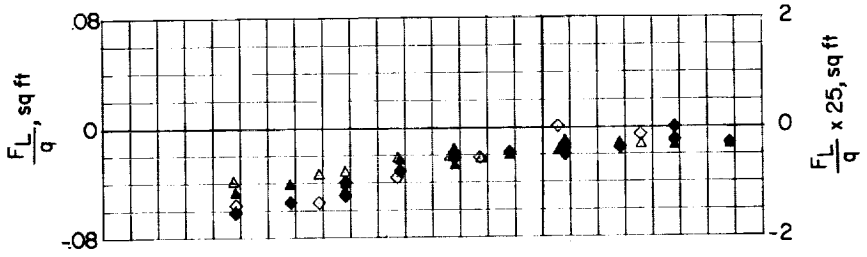

(b) Lift.

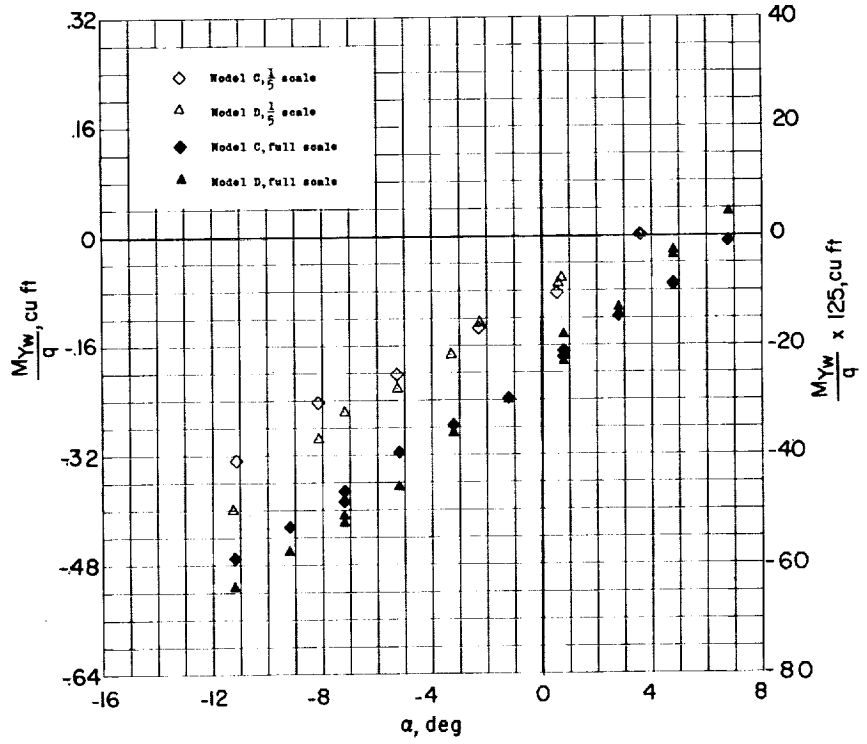

(c) Pitching moment.

Figure 28.- A comparison of $\frac{1}{5}$-scale and full-scale results for models C and D. Tunnel stream angle corrections have been applied.